4.4. Statistics of Freja charging events

4.4.1 Amount of data and charging characteristics

This statistical study includes 291 charging events found in the time period October, 1992, to May, 1994. All ephemerid data up to orbit 10,000 were used for normalisation of the statistical data presented below. Five evenly distributed occasions were selected from each orbit for which orbit number, date, altitude, corrected geomagnetic latitude (CGLAT), magnetic local time (MLT), longitude and universal time (UT) were extracted. Only occasions where real data existed were kept for the normalization.

Most of the charging events were low level charging events, i.e. peak charging below 10 V (Figure 4.4-1). However, a few of the Freja charging events reached larger potentials than –2000 V. The duration of the main part of the Freja charging events (Figure 4.4-2) were shorter than one minute, but a few lasted several minutes.

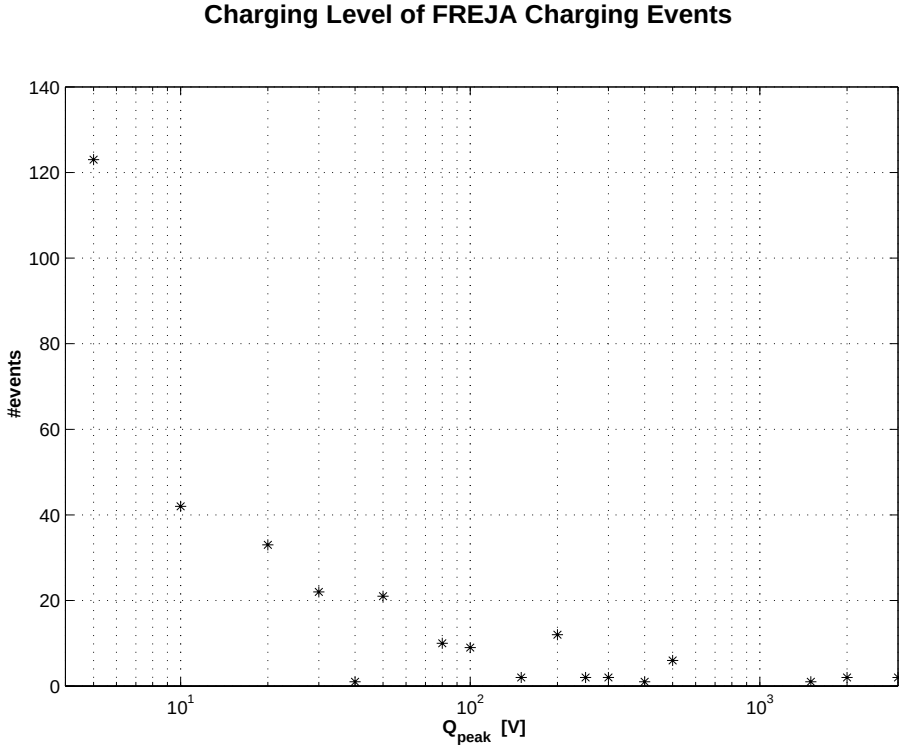

Figure 4.4-1: The charging level distribution.

The charging levels were 2–3 times larger than those reported from the DMSP F6 and F7 satellites traversing an altitude of 840 km (see e.g. Gussenhoven et al., 1985; Stevens and Jones, 1995). This is somewhat remarkable, because the Freja was designed to be as conductive as possible and therefore should be much harder to become charged. On the other hand, Freja traversed higher altitudes and therefore lower plasma density regions, a physical parameter that has been suggested to be of importance for surface charging (Frooninckx and Sojka, 1992). Also, the Freja charging levels were well below the maximum charging levels detected on spacecraft in GEO, such as the ATS-5, ATS-6

and the SCATHA (P78-2) satellites (e.g. Mullen et al., 1986; Olsen, 1983), where charging levels of several thousand volts are achieved.

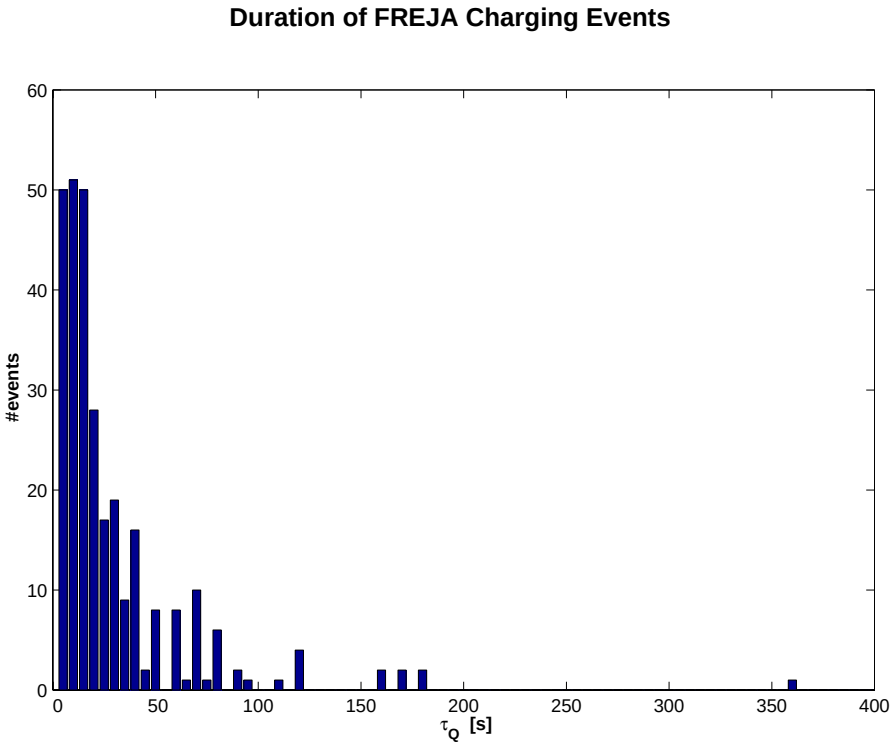

Figure 4.4-2: Duration of charging events.

4.4.2. Variation with sunlight conditions

The Freja charging events were distributed with respect to sunlight conditions according to the following:

- 32 events occurred during sunlight
- 236 events occurred during eclipse
- 23 events occurred close to the terminator

Most Freja charging events occurred during the dark winter months as can be seen in Figure 4.4-3, where the periods between November and February host most of the Freja charging events. The sunlight events (dark portion at bottom of bars) were possibly more spread out over the year, but no events were detected during the summer months.

4.4.3. Variation with geomagnetic location

The variation in Magnetic Local Time is presented in Figure 4.4-4. Freja charging events occurred clearly during nightime hours with an event peak around 22:00–23:00 MLT. Almost no charging events were found between 06:00 and 18:00 MLT. Thus most charging events occurred in the absence of the photoelectron emission from the space-craft. We want to stress that this is not an effect due to the fact that charging events only occur in certain latitude or longitude regions because all MLT zones were covered rather evenly by the Freja orbits.

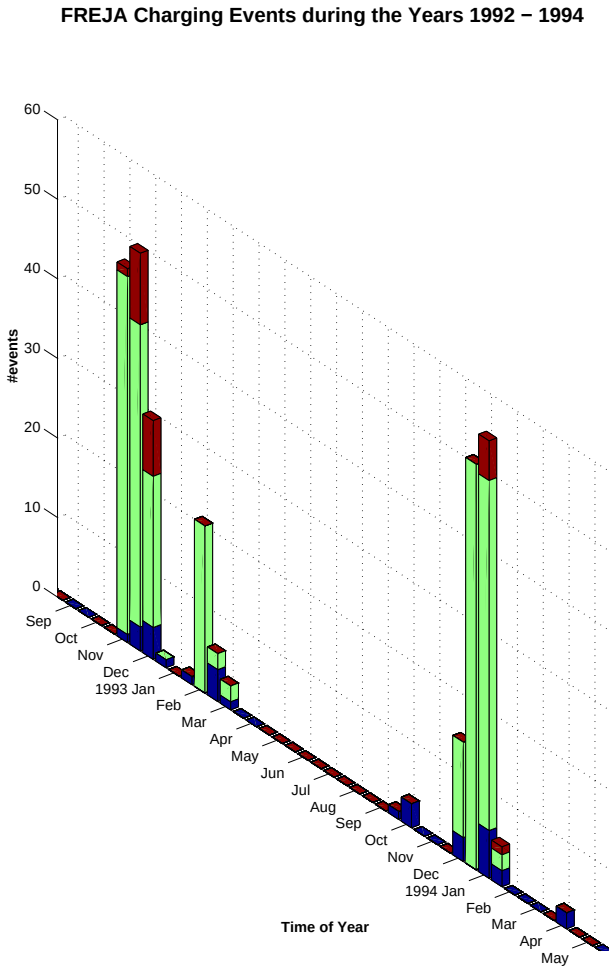

Figure 4.4-3: Seasonal dependence.

The variation in Corrected Geomagnetic Latitude is presented in Figure 4.4-5. Freja charging events were restricted to latitudes above 60°. The charging event frequency seems to decrease at geomagnetic latitudes above 70°. Clearly, all Freja charging events occurred within the auroral zone.

The variation in Longitude is presented in Figure 4.4-6. Except for the two events near –155°, the distribution is contained to –140° to –30° longitude. This is just due to a latitudinal effect, since large enough latitudes was only reached inside this longitude range. Of course, very active conditions (large Kp index) and keV electron precipitation is expected within the auroral zone as will be further shown below.

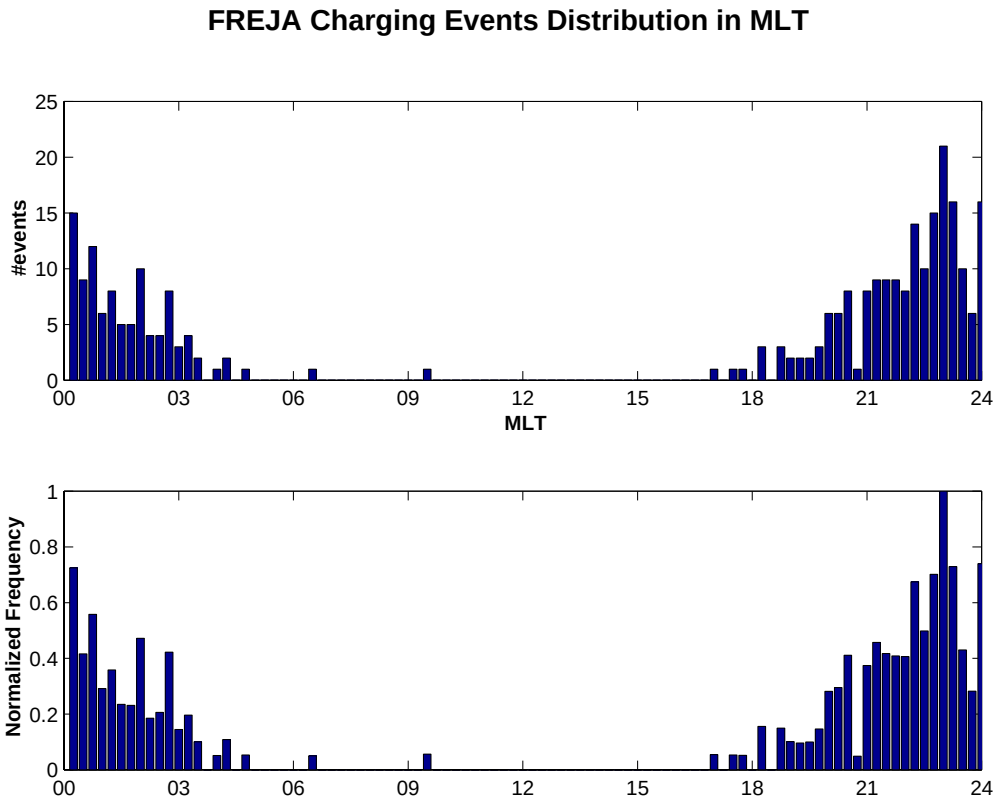

Figure 4.4-4: Variation in MLT.

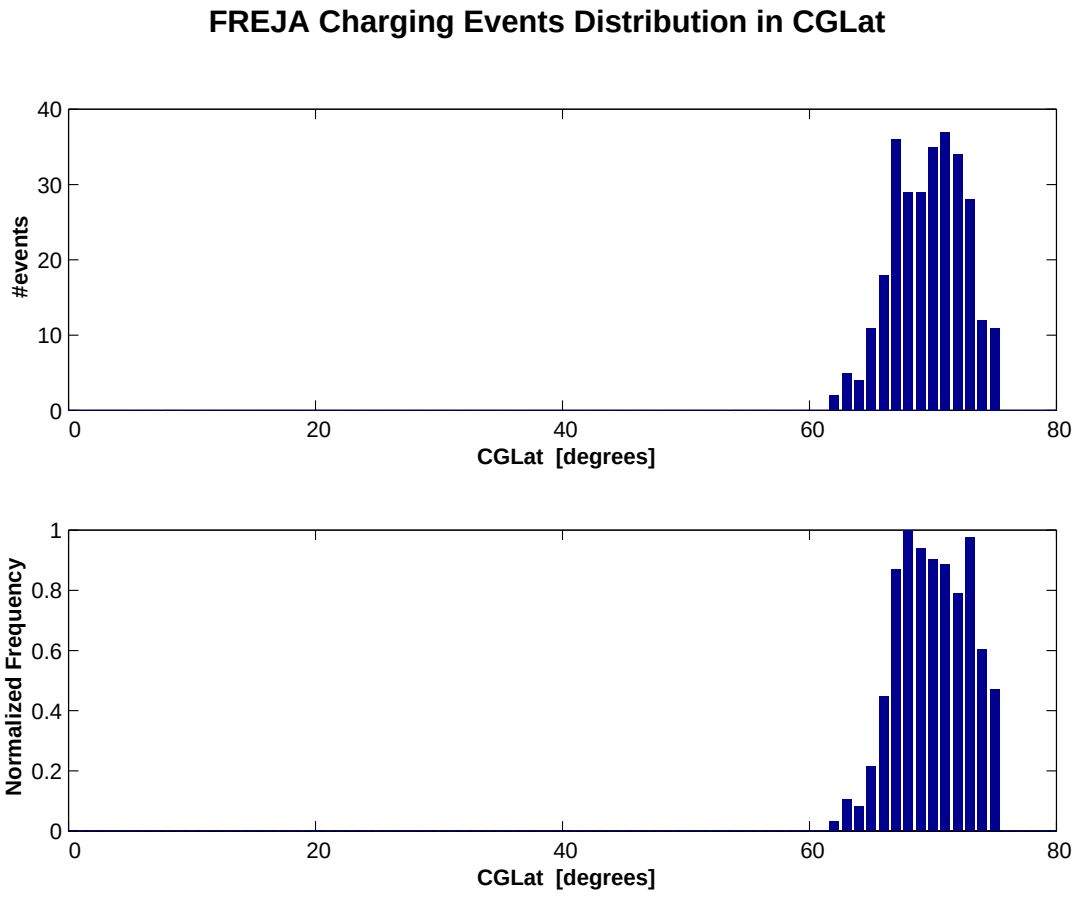

Figure 4.4-5: Variation in CGLAT. Freja covers latitudes down to 40°.

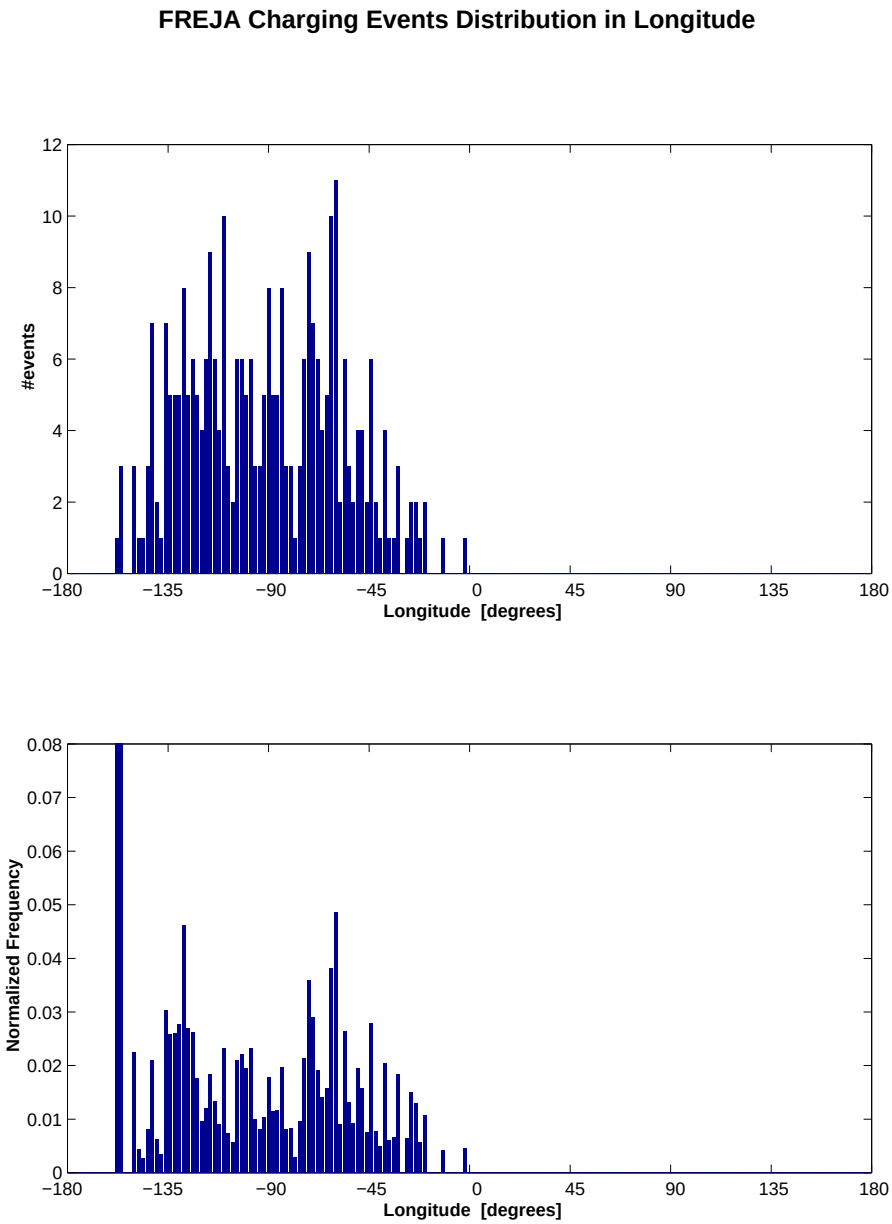

Figure 4.4-6: Variation in longitude.

4.4.4. Variation with geomagnetic activity

The Freja charging events have been binned to fit the 3-hour averages of the global Kp index, an indicator for geomagnetic activity. The bottom panel of Figure 4.4-7 shows the normalisation used for the Freja time period, the middle panel shows the normalised results for the Freja charging events. We can note that

- there is a weak increasing tendency with increasing Kp index
- the probability of charging becomes large for Kp > 3+.

These results agree fairly well with the results of Mullen et al. (1986), based on geostationary SCATHA data, while only a weak correlation was obtained with the DMSP satellites in LEO orbit (Frooninckx and Sojka, 1992).

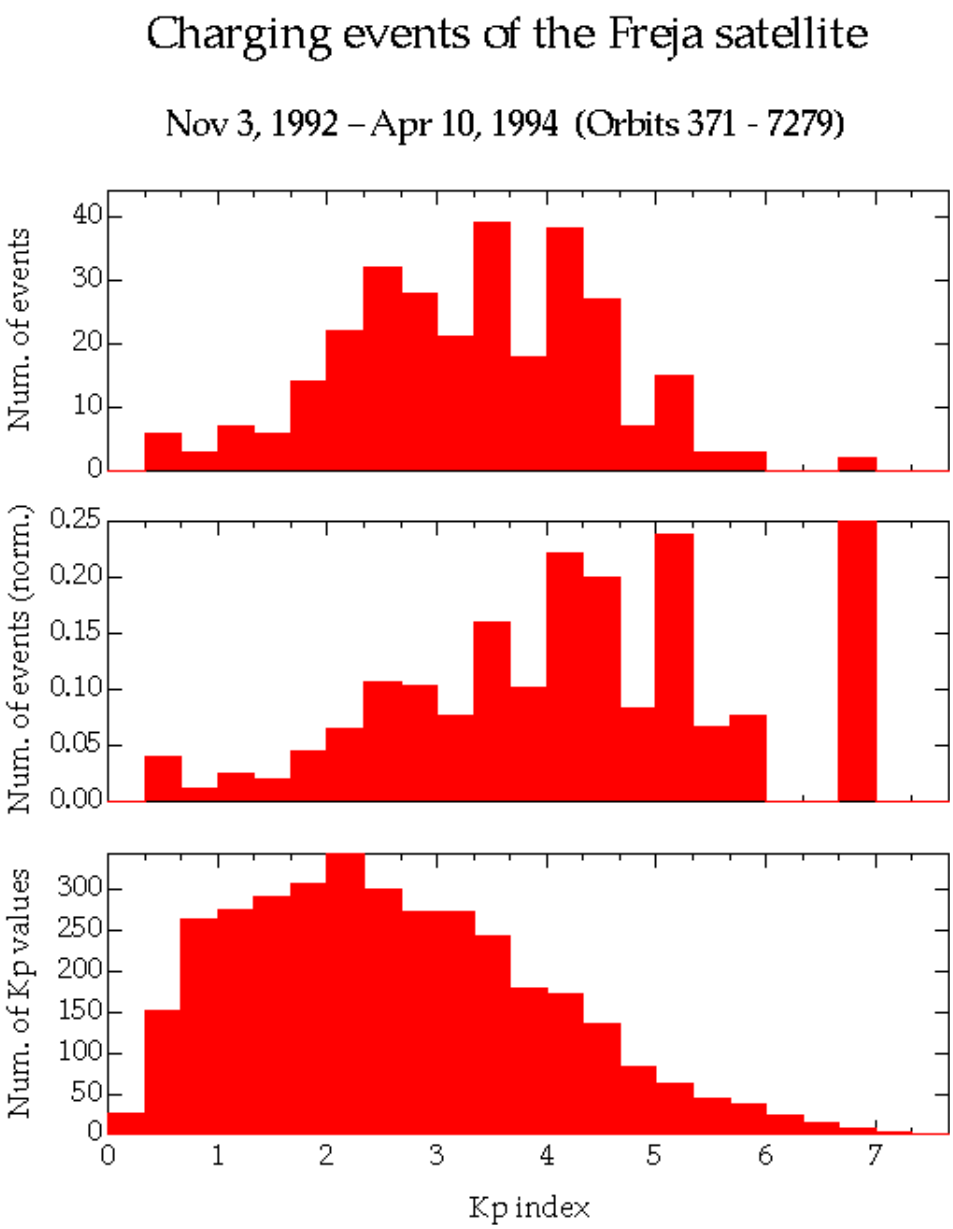

Figure 4.4-7: Variation in geomagnetic activity level (Kp).

Figure 4.4-8 shows the charging events were distributed in Kp for different MLT, altitude, and sunlight conditions. The data points in the eclipse index have been shifted randomly in order to highlight the distribution of events with sunlight conditions better. We can note that

- low Kp events tended to occur in a narrow local time sector near local midnight (panel a)
- high Kp events happened within a broader local time sector on the nightside, although the Freja spacecraft did not need be in shadow (panel a compared to panel b)
- low Kp events occurred only during eclipse (panel c)
- no obvious dependence with altitude is found

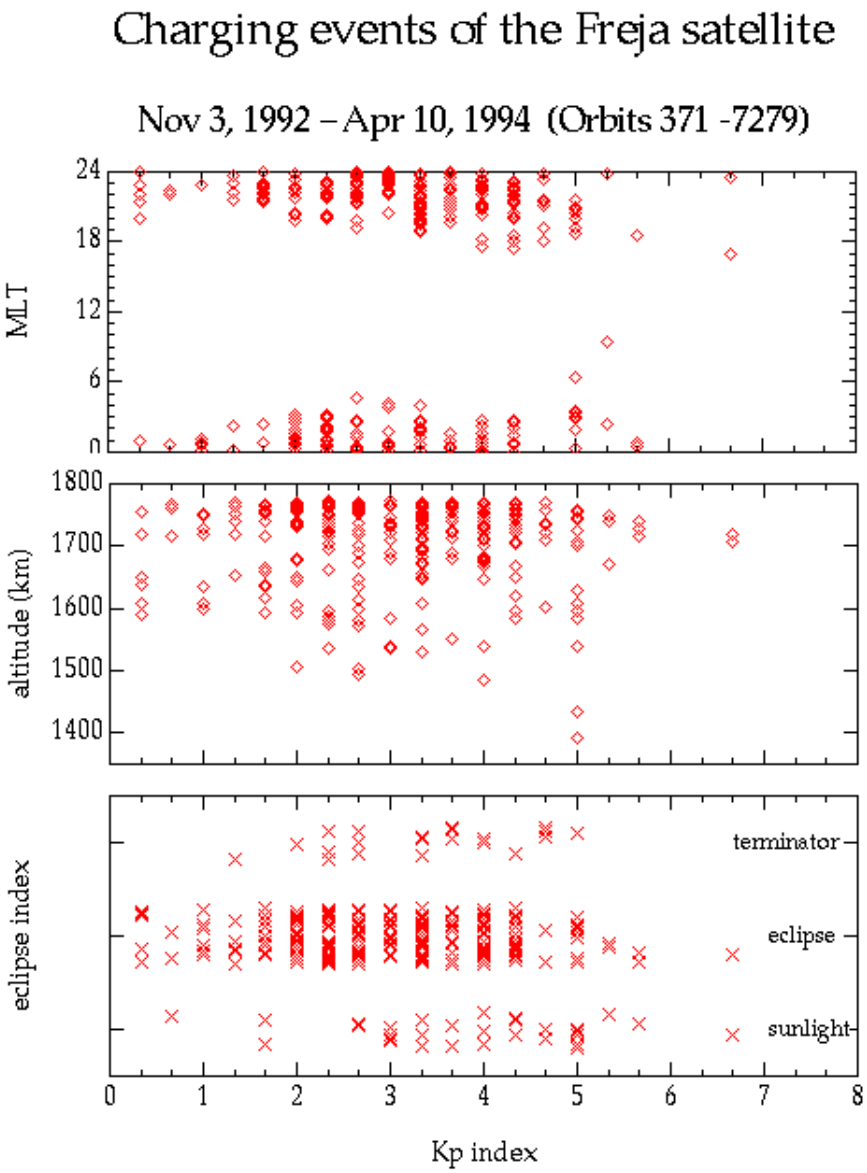

Figure 4.4-8: Variation of Kp with respect to MLT, altitude, and sunlight conditions.

4.4.5. Variation with cold plasma characteristics

Figure 4.4-9 (panel a) shows the peak charge variation with electron density. Here, the peak charge values have been slightly randomised (10 %) to highlight the dependence better. Unfortunately, no clear relationship is obvious. However, there is an upper threshold value of $2 \cdot 10^9$ m^{-3} for the cold plasma density, since it is well known that the cold plasma density often reach above this value in the Freja data. The thermal plasma density seldom decreases below 10^8 m^{-3} in the Freja dataset.

This result can be compared with the results obtained by Frooninckx and Sojka (1992), who found a similar electron density threshold value of 10^{10} m^{-3} for the DMSP satellites. Since the DMSP satellites traversed lower altitudes (840 km) and therefore larger thermal plasma densities, this result confirms that the Freja spacecraft was indeed

better designed with conductive surface coatings for electrical cleanliness. Despite this fact, Freja nevertheless charged more than 2000 Volts negative.

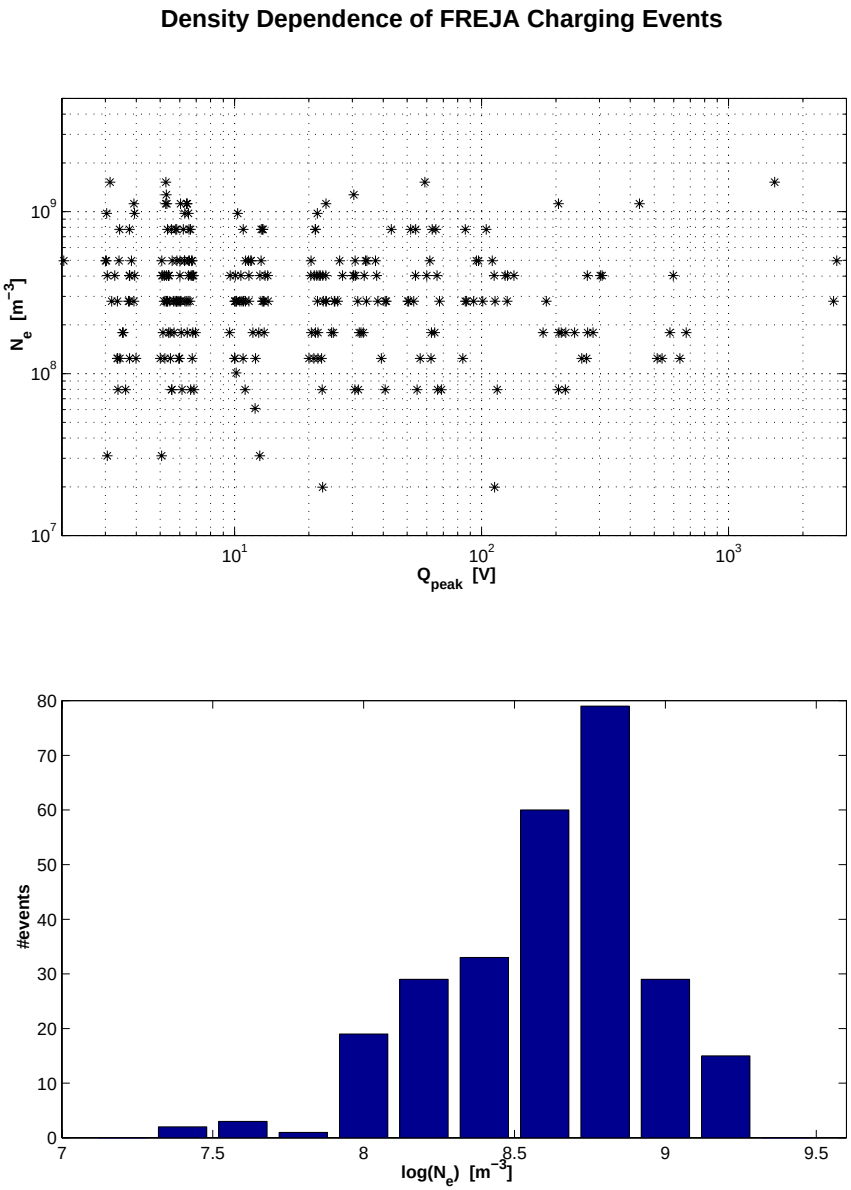

Figure 4.4-9: Variation in the cold ambient plasma density.

4.4.6. Variation with energetic particle characteristics

By far the most common type of Freja charging events was associated with energetic electron precipitation in association with inverted-V events. It is fair to conclude that the energetic electrons with energies above a few keV were the direct cause for most Freja charging events. Figure 4.4-10 shows an avaraged electron spectrum for all Freja charging events, where a clear inverted-V electron population with a peak energy of few keV and an extended power-law type high-energy tail extending to several tens of keV can be seen. Typical flux levels at the inverted-V energy peak during charging events reached 5×10^{11}–10^{13} $(m^2\text{-s-str})^{-1}$ for single charging events.

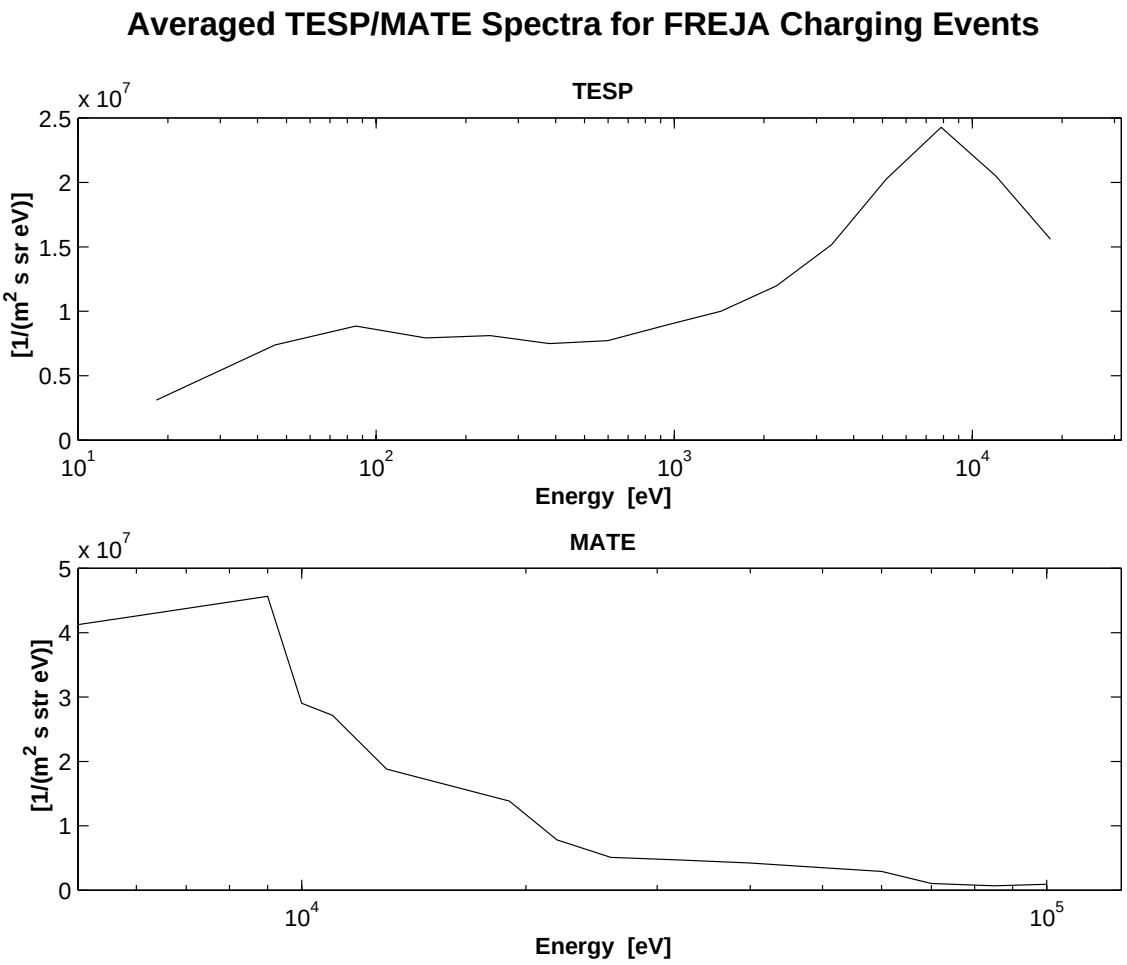

Figure 4.4-10: Averaged electron spectra for all Freja charging events.

The relationship of spacecraft charging can be further demonstrated by looking at the averaged electron spectra for different charging levels (Figure 4.4-11). It is clear from Figure 4.4-11 that both the inverted-V peak energy and flux as well as the high energy tail flux were increased for higher charging levels. A second peak seemed to exist between 10–100 keV, which becomes more pronounced at larger charging levels. Note also that no significant electron fluxes are seen at lower energies (< 1 keV). Such electrons would increase the secondary yield and inhibit charging on Freja, because ITOC is the main surface coating on Freja and because ITOC has a break-even point with respect to secondary electrons near 2.5–3 keV. The second most common surface material is the thermal blanket, which has the break-even point just below 4 keV. The results are therefore in qualitative agreement with normal surface charging theory (e.g. Garrett, 1981; Hastings, 1995; Hastings and Garrett, 1996).

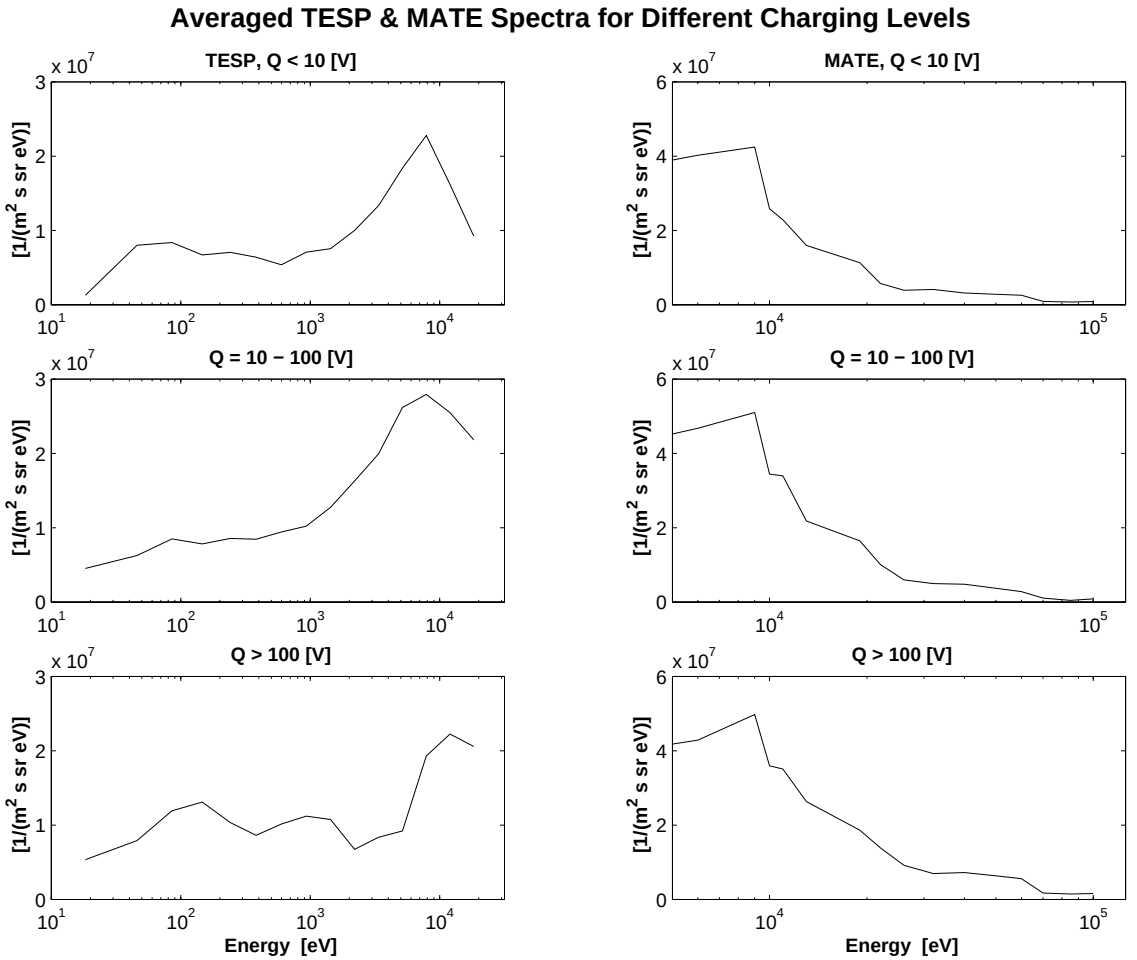

Figure 4.4-11: Variation in electron spectra with respect to different charging levels.

Frooninckx and Sojka (1992) showed that the thermal plasma density is one of the major factors determining the charging level of the DMSP spacecraft. We show in Figure 4.4-12 the counting rates for a selected number of fixed electron energy levels (for the MATE instrument) plotted vs the peak charging level. As expected, no sensational relationship can be found. It is obvious that the high energy electron flux *alone* is not a major physical parameter for determining the charging level of Freja. If we instead divide the flux (count rate) with the cold plasma density, as Frooninckx and Sojka (1992) did, a somewhat better (still bad) relation appears. However, a rather good relationship is obtained near the peak energy (around 4.3 keV) if we also divide the flux with the flux at the lowest energy channel (794 eV, Figure 4.4-13). This low-energy flux is well below the break-even energy for secondary electrons emitted from the surface, and the larger this flux is the lower charging level we expect. A high energy electron flux level is indeed needed, but it seems that other physical parameters, such as the thermal plasma density (and the return current from this plasma to the spacecraft) and the low energy electron flux (which produce many secondary electrons) determines the charging level to a great extent as well. A somewhat better dependence therefore is seen in Figure 4.4-13. Thus the following relationship seems to roughly hold:

$$Q \propto \left(\frac{\Phi_{peak}}{\Phi_{low} \cdot n_e} \right)^{1.5}$$

where Q is the charging level attained, n_e, the thermal plasma density, Φ_{peak}, the electron flux at the inverted-V peak energy, and Φ_{low}, the electron flux at low energies (e.g. around a few hundred eV).

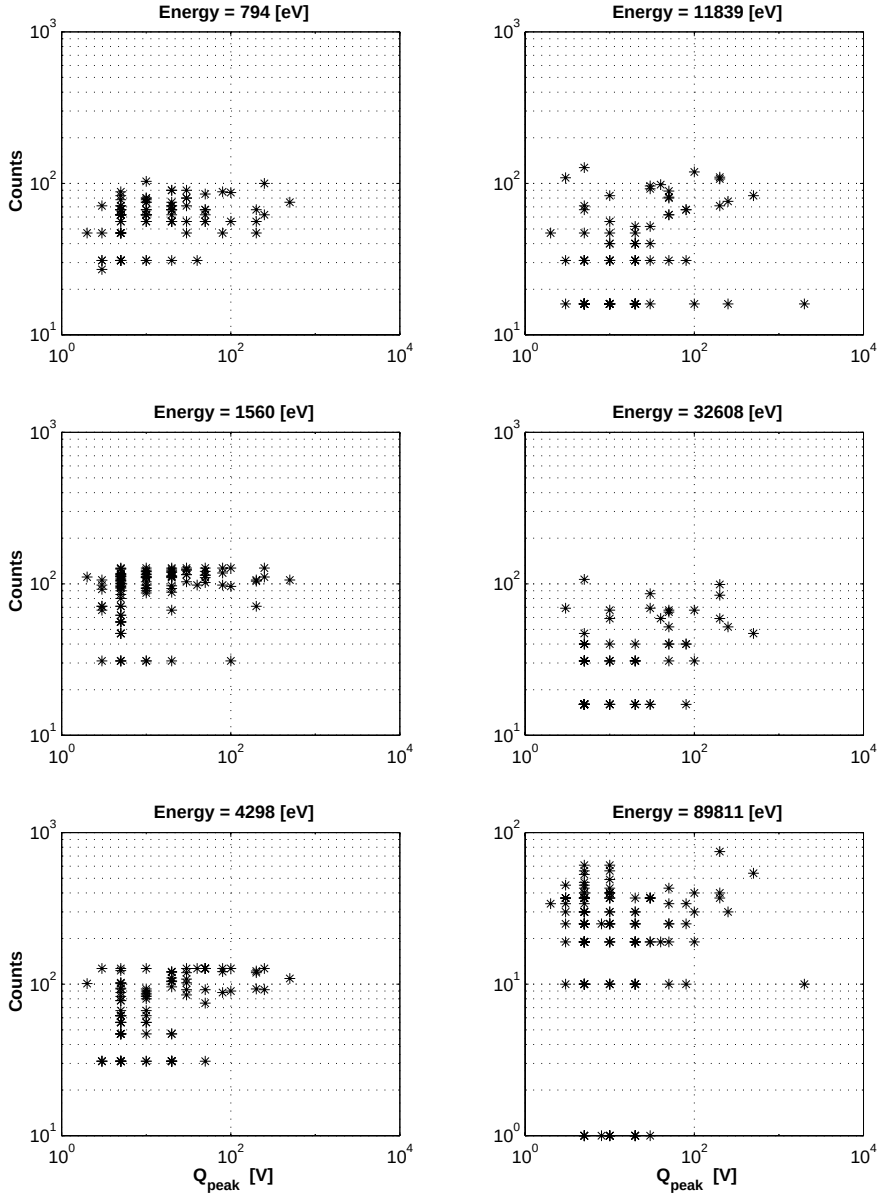

Figure 4.4-12: The count rate (flux) for a selected number of fixed electron energy levels (from MATE) plotted vs the peak charging level.

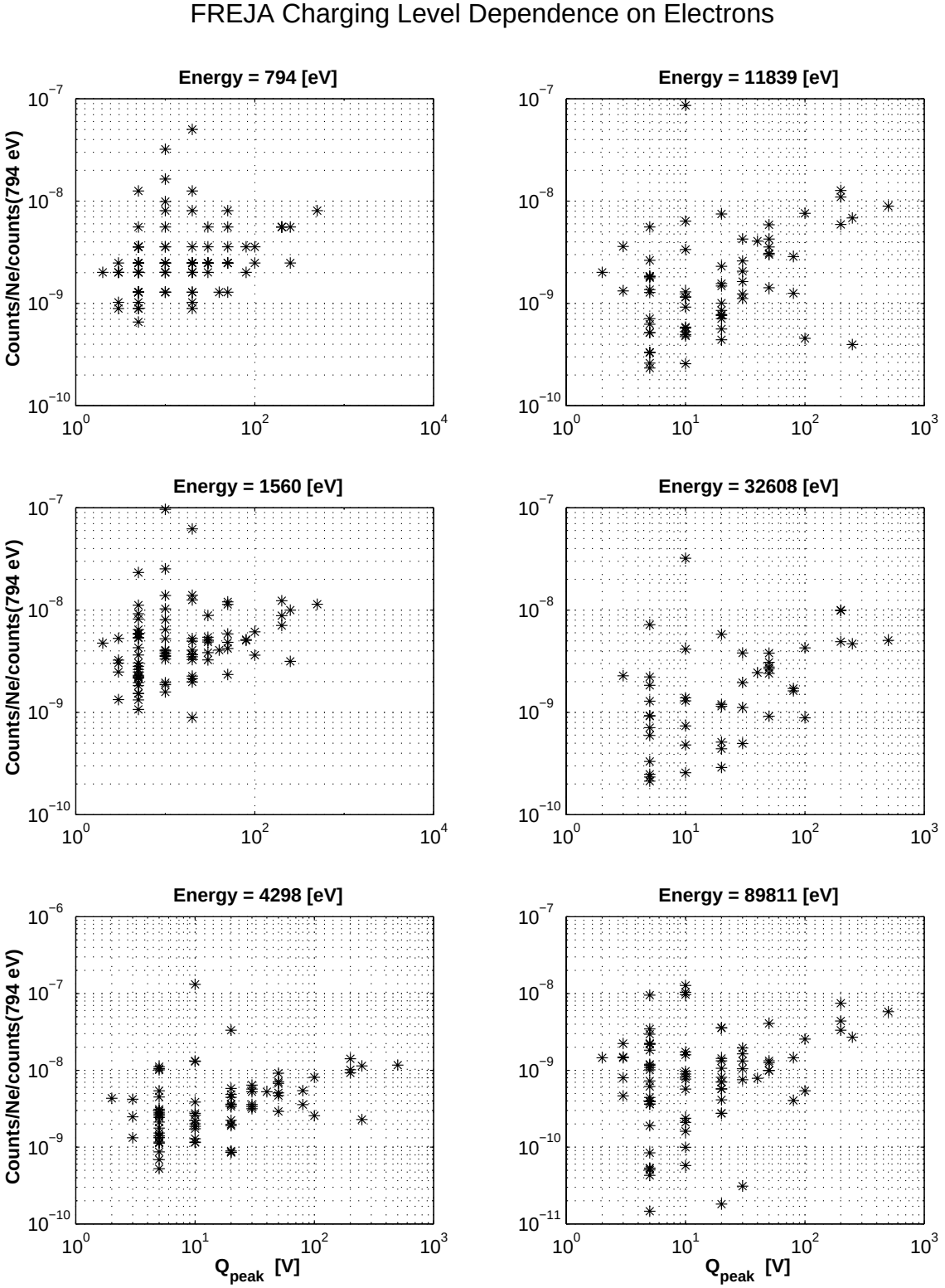

Figure 4.4-13: The magic formula. The low energy electron flux is an inhibiting charging factor, since it produces relatively large amounts of neutralising secondary electrons. The larger the density, the harder it is to charge a spacecraft because of increasing the neutralising thermal ion current. Above a certain threshold energy, the flux near the inverted-V energy peak carry a net negative charge to the spacecraft (less backscattered and secondary electrons). There is a good relationship near the inverted-V peak energy (first column, bottom panel).

4.4.7. Variation with altitude and magnetic field strength

The distribution of Freja charging events with altitude is displayed in Figure 4.4-14. The normalised altitude occurrence of charging events (panel b, although "noisy") seems to be rather evenly distributed. Perhaps there is an increasing trend for increasing altitude, but this trend is within the possible errors.

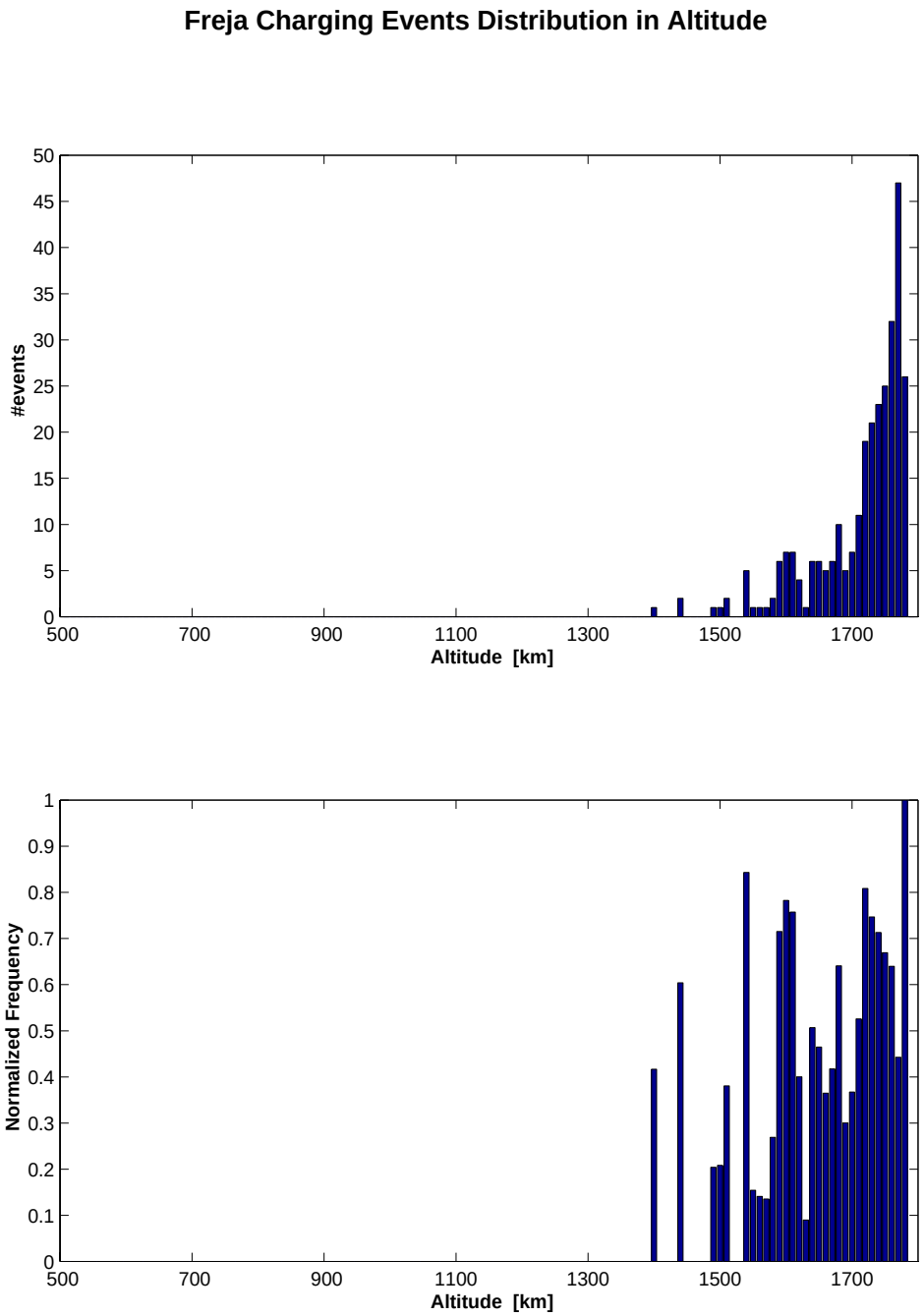

Figure 4.4-14: Variation in altitude.

In low Earth orbit, the geomagnetic field **B** is strong enough that secondary electrons and photoelectrons emitted from the spacceraft surface have an average gyroradius smaller

than typical dimensions of a spacecraft. For Freja conditions these dimensions are comparable. This implies that escape of such electrons may be inhibited on surfaces nearly parallell with **B**, which in turn may affect the current balance of the spacecraft and make high-voltage charging more likely (Laframboise, 1988). The effect of the Freja orientation with respect to the magnetic field direction was therefore investigated. Figure 4.4-15 displays the dependence of the Freja spin axis angle to the magnetic field direction. There is an apparent increase of charging events at smaller magnetic field angles (panel b). However, this is just a latitude effect. Figure 4.4-16 further shows that no obvious dependence exists between charging level and magnetic field direction in the Freja dataset. We conclude that the magnetic field orientation was not a major factor for charging of the Freja satellite.

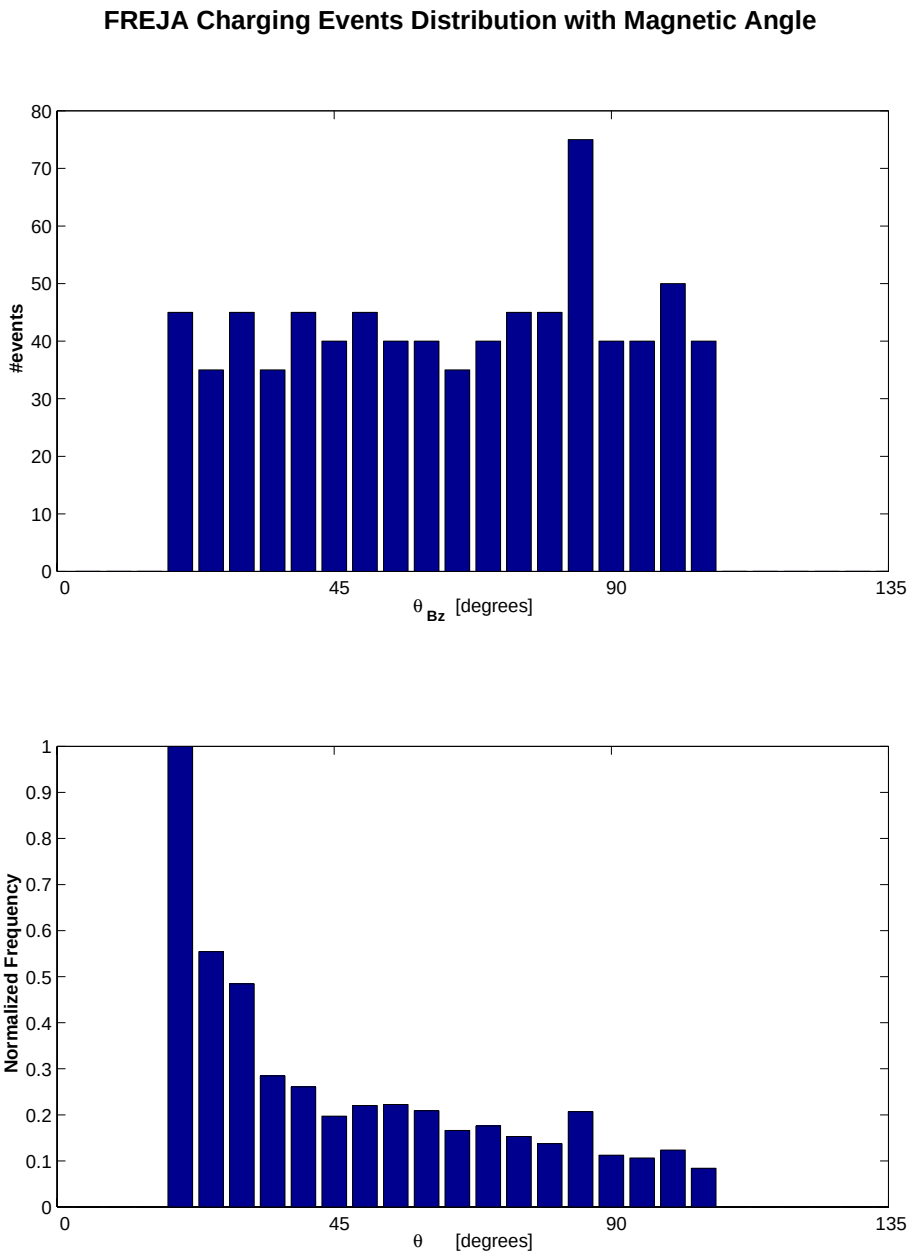

Figure 4.4-15: Dependence of Freja's orientation with magnetic field direction. The apparent increase toward smaller angles is unfortunately only a latitude effect.

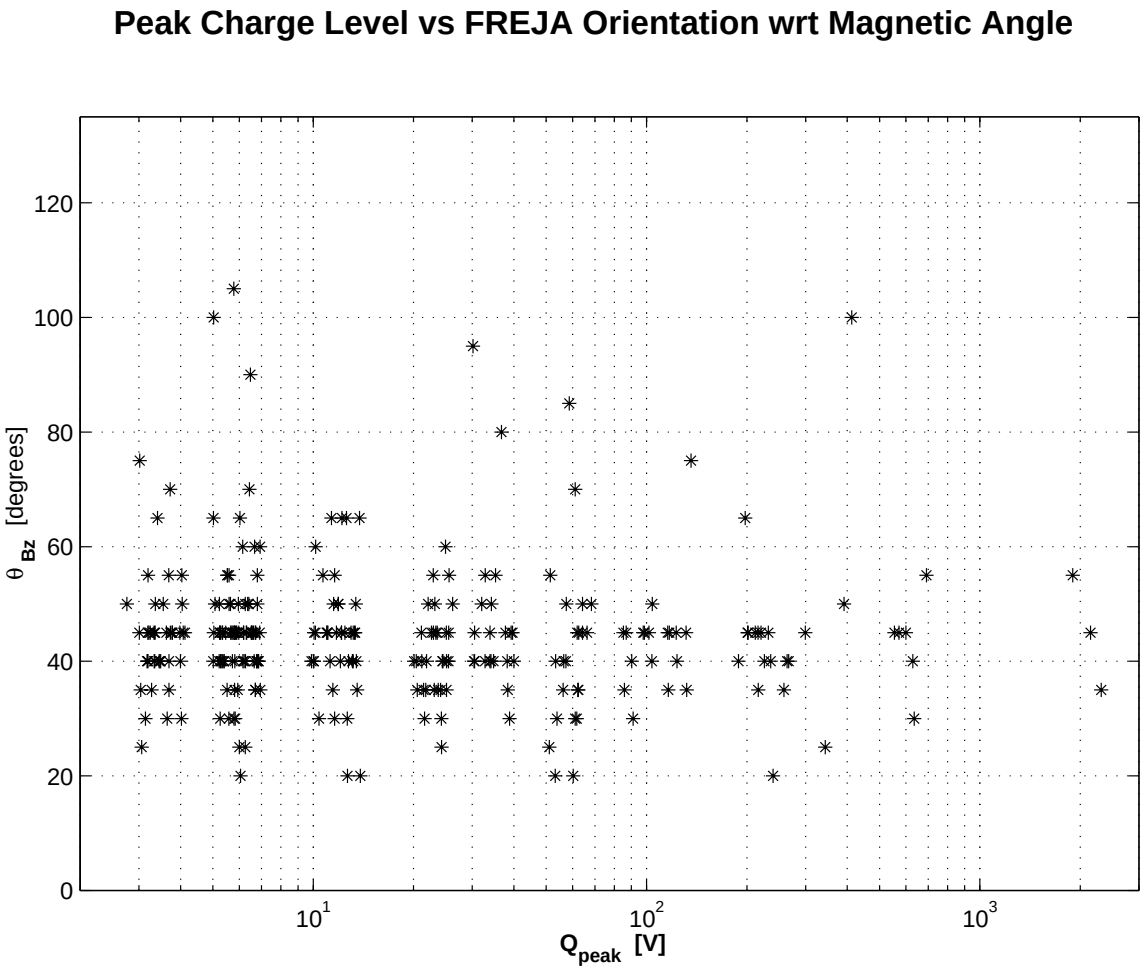

Figure 4.4-16: Dependence of charging level with geomagnetic field direction.

4.4.8. Conclusions regarding to Freja charging statistics

By far the most common type of charging detected on the Freja satellite occurred during high-latitude auroral inverted-V events when extreme fluxes of high energy (5–80 keV or more) hit the spacecraft. Usually the cold ambient plasma density was low ($<1\times10^9$ m^{-3}) during the events, and a majority of them occurred during eclipse. All charging events can be classified in four different types:

- Charging by energetic electrons during eclipse
- Charging by energetic electrons during sunlight and terminator conditions
- Low level charging variations due to sunset/sunrise.
- Low level charging probably due to an increased bulk electron temperature.

The last two types of charging usually remained to levels below the threshold we have chosen for this statistical study, and therefore only few such events were included.

Based on the data sampled on 291 orbits we can draw the following conclusions:

- Most charging events did not reach charging levels in excess of 10 V (negative). Only a handful of the events reached charging levels around –2000 V.

- The duration of the charging events were mostly shorter than one minute. Only very few lasted several minutes even though Freja had an orbit that passed almost tangentially along the auroral oval. This fact reflects the passage time over so called inverted-V structures within the auroral region (i.e. bursty events of precipitating high energy electrons). Thus, when the source for charging disappears, the charging disappears simultaneously. This is confirmed by the results from the event study (section 4.3 above).
- All charging events occurred only above Corrected Geomagnetic Latitudes of 60° with a frequency peak centred above the auroral zone.
- The geomagnetic activity as measured by Kp needs to be larger than 2+ for charging events to be probable and the probability increases for larger Kp.
- Typical inverted-V electron differential fluxes are 10^6 to 10^8 $(cm^2\text{-s-str-keV})^{-1}$. Examples of worst case electron spectra were presented in section 4.3. However, the ambient plasma density, sunlight conditions and the energy of the inverted-V peak affect the charging levels more dramatically. Also, electrons at energies around a few hundred eV, for which the surface secondary yield is the largest, appear to inhibit negative charging.
- No Freja charging events occurred for thermal plasma densities above $2 \cdot 10^9$ m^{-3}. DMSP had a threshold value of 10^{10} m^{-3}. The larger density increases the neutralising thermal ion return current to the spacecraft.
- The electron spectra show low flux levels below about 1 keV, and larger flux levels above a few keV. The spectra seem to have two populations, one with peak energies of a few keV, and one high energy tail between 10–100 keV.
- Most charging events occurred during the absence of photoemission from the Freja spacecraft (i.e. in eclipse), and enhanced negative charging levels were obtained during sunlight only during very active auroral conditions (Kp > 2–3).
- No charging events occurred during the summer months, while a maximum of occurrence appeared in the winter months. This is probably due to the combined effect of increased eclipse time and the expected lower thermal plasma density in the absence of photo-ionisation and the upward diffusion at lower altitudes.
- Most charging occurred in the MLT interval 18 pm – 03 am.
- No obvious relationship was detected regarding the orientation of the Freja spin axis with respect to the geomagnetic field direction even though the electron gyroradius of the photoelectrons and secondary electron emission from the spacecraft surface and the dimensions of Freja are comparable.

It is worrisome that an electromagnetically clean spacecraft where the designers have made special effort to provide conductive surfaces still gains charging levels of several thousand volts negative during auroral active conditions. The main surface material on Freja was ITOC, which has a cross-over energy of about 2.5–3 keV, above where the secondary yield falls below 1. The second largest surface type was covered by thermal blankets with a slightly larger secondary yield crossover energy of just below 4 keV. The spectral characteristics of a typical auroral inverted-V events with insignificant low-energy

fluxes (< 1 keV) and large fluxes of high energy electrons (often isotropically distributed in pitch-angle) make these events particularly effective in producing high charging levels on *any spacecraft* where the secondary yield crossover energy for the surface material is a few keV. Highly conductive surface materials are needed to avoid differential charging problems among different surfaces on a spacecraft, but if a total charging of a polar spaccraft shall be avoided, then the surface materials need have secondary yield crossover energies of at least 20–30 keV, which seems impractical.

The gyroradii at Freja/DMSP altitudes for around 2 eV secondary electrons are 0.1–0.4 m, which is a significant fraction of the size of Freja. Even so, only very few of these electrons will return to Freja through gyromotion, depending on orientation with respect to the Earth's magnetic field direction (Laframboise, 1988). For a larger spacecraft a larger fraction of these secondaries will return to the spacecraft surface, and a larger spececraft will thus likely gain even higher charging levels. The same argument is true with regard to sunlight conditions, when large amounts of photoelectrons are emitted from the surface. A smaller spacecraft will not see the photoelectrons return as easily as a larger spacecraft, and the larger spacecraft is therefore more easily charged.

We make the conclusion that high level surface charging will continue to occur on spacecraft in PEO, and that it will require serious engineering efforts to produce surface materials with large secondary yields for incident electron energies in excess of tens of keV but which are still conductive. Of course, indirect methods to reduce charging levels exist, like expelling a cold rather dense plasma around the spacecraft, but such methods instead tend to increase the contamination and differential charging problems. Problems which will affect the performances of scientific instruments onboard these spacecraft.

4.5. Numerical modelling of Freja charging observations

In this section we discuss the modelling of Freja charging events using the numerical spacecraft charging codes SUCHGR and POLAR. As explained above the Freja instrumentation makes it possible to experimentally study bulk charging of the spacecraft, and this is what is modelled here. Differential charging as such is not a chief consideration in this work as no observational Freja input exist, but some effects of local electrostatic perturbations are investigated.

From discussion in sections 4.3. and 4.4. it is clear that voltage levels below the expected floating potential, as based on the thermal plasma characteristics, often are observed on Freja. It was also shown that the spacecraft potential in these cases is closely correlated to electron precipitation above some keV. In thissection we attempt to model these results using SUCHGR and POLAR, briefly presented in subsection 4.5.1. Our approach is that of an "un-prejudiced best-effort": we first describe the spacecraft (4.5.2) and its surface materials, then model it (4.5.3) and its environment (4.5.4) as accurate as possible, and finally use this as input to POLAR, the code developed to deal with auroral charging phenomena in low-Earth orbit. For the simulations (4.5.5), we use POLAR version 1.3.7, kindly provided by David Cooke of the US Air Force Research Laboratory.

We find that POLAR used by us in this way does not reproduce the observed charging levels, although variation of material or simulation parameters sometimes get us close to observed voltages. Possible reasons for the discrepancies are discussed, and we conclude this study with a summary and recommendations for further investigations and software development in subsection 4.5.6.

4.5.1. Modelling spacecraft charging

4.5.1.1. Spacecraft charging codes

Several software tools for modelling spacecraft surface charging exist. Most well known and commercially available is the NASA Charging and Analysis Program, NASCAP, developed in the USA in 1980s. For the study of charging effects on satellites in polar orbits, the code POLAR was developed from NASCAP in the late 1980s. POLAR has additional capabilities to model the auroral electron precipitation, which is the essential source of spacecraft charging on polar orbits. In Russia, the ECO-M and COULOMB codes have be developed (e.g., Danilov et al., 1998; Krupkinov et al., 1992). Common to these and most other spacecraft charging codes is that they use quasi-analytical models for some parts of the calculations, for example for the wake structure, rather than doing a complete particle-in-cell simulation or numerical solution of the Vlasov-Poisson equations for the spacecraft-plasma system. There are 2D particle-in-cell for charging studies codes (e.g. Usui et al., 1993) and 3D codes are under development, but at present only the semi-phenomenological codes mentioned above are widely available and applicable in practical situations.

POLAR has previously been applied, e.g., to the SPEAR-1 rocket (Katz et al., 1989), the CHARGE-2 rocket payload (Mandell et al., 1989), and to the DMSP series spacecraft (Cooke et al., 1989). For modelling of Freja charging events, typically at around 1500 km altitude in the auroral zone, POLAR was chosen as the most appropriate tool presently available, although NASCAP was used as well in some preliminary work (Svensson, 1997). We have also used the program SUCHGR which is distributed with the POLAR code. SUCHGR is a simplified code modelling the spacecraft as a homogeneous sphere, while POLAR allows detailed modelling of the spacecraft. POLAR and SUCHGR are described in detail in the POLAR User's Manual (Lilley et al., 1989, hereafter refered to as PUM). In the context of the present study it is necessary to have some knowledge of what POLAR can do and what it cannot, as this clearly is important for understanding the results of the simulations of the Freja charging events.

4.5.1.2. Currents collected from the plasma

The currents flowing to an isolated body in a plasma depend on the potential of the surface with respect to the surrounding plasma. Under all conditions, the body will attain a potential V such that the total current I is zero. The presence of non-conductive materials, which may give local charging to parts of the spacecraft, or biased parts like scientific in-

struments for particle collection, may perturb the electrostatic field around the spacecraft. Denoting the equilibirum potentials of surfaces k by V_k the spacecraft boundary to space will be such that the total current is zero

$$\sum_{k=1}^{n} I_k(V_1, V_2, ..., V_n) = 0 \quad . \tag{4.5.1}$$

This is the fundamental equation of spacecraft charging. For simple models like a homogeneously conductive spherical spacecraft of uniform surface it may sometimes be possible to give closed-form expressions for *I(V)*, although the presence of shielding and particularly wake effects make the problem hard to solve (see Al´pert, 1983). The code SUCHGR uses this simple model. For a uniformly conductive spacecraft, results based on such simplifications may often be very good, particularly if the Debye length is large compared to spacecraft dimensions. In other cases, where a spacecraft with many different surfaces and a complicated geometry is to be considered or wake effects are important, more elaborate calculations are needed. Codes like NASCAP and POLAR divide the satellite into a set of surfaces, each satisfying a current balance equation similar to (4.5.1), where I and V are vectors describing the currents and potential for each surface. In general, the current to any surface depends not only on its own potential but also on the potentials of the adjacent surfaces and the spacecraft bulk, as these potentials will influence the particle motion in the plasma and the current flow on the spacecraft.

For modelling a spacecraft-plasma interaction problem with negative charging, POLAR typically starts from user-supplied input on the spacecraft geometry and materials, the plasma parameters and initial potential of the spacecraft. An initial wake structure is determined using geometric shadowing of the spacecraft or a neutral flow approximation. An initial sheath edge is fixed, and using these boundary conditions Poisson's equation for the potential is solved. The motions of test ions are then tracked through the field, and the currents they carry to the spacecraft surfaces are calculated. The currents and densities due to the repelled electrons are calculated using the Boltzmann relation. The response of the spacecraft surfaces to the incoming particle flux is calculated, resulting in a new potential distribution on the spacecraft. This is then used as a new boundary condition for Poisson's equation, which is solved with the ion density found from the tracking process and Boltzmann distributed thermal electrons providing the charge density. Contributions to the charge density from high-energy electrons, secondary electrons, photoelectrons and backscattered particles are not modelled.

If the plasma is sufficiently tenuous, the electric fields encountered by the particles can be determined from the boundary conditions without reference to other particles in the plasma. In this limit where the Debye length is much larger than the spacecraft size, fields will also decay with distance so slowly that the current is independent of the detailed structure of the field. This is known as the orbital motion limit or OML, for which useful analytical results exist (Mott-Smith and Langmuir, 1926; Medicus, 1962). At the other extreme, in a plasma so dense that the Debye length is much smaller than the spacecraft size, a sheath may form and shield off potentials so effectively all particles that enter the sheath are absorbed. Also for this limit, the sheath limit, some exact results exist (Al´pert, 1983). In between the extreme levels we have a situation which we may call the space

charge limited current collection, which is where the scheme described in the preceeding paragraph is needed.

Evidently, the space charge limited case is more complicated to handle than OML. However, one may note that outside the sheath edge, OML conditions always apply. If detailed tracking of particle orbits is needed, this has to be done only inside the sheath. This is utilised in POLAR, which switches from OML relations to detailed particle tracking at a presumed well-defined sheath edge, defined by default as $|\Phi| = 0.47\, KT_e / e$. POLAR also has the option of using OML theory only and skip detailed particle tracking. Finally there is a hybrid of the two built into POLAR, where the OML calculation is done for finding the distribution of currents on different parts of the spacecraft, whereafter the total current to the spacecraft is normalized to the sheath current. This approach significantly reduces the amount of calculations as compared to the detailed particle tracking in the sheath, but its usage is not well tested or documented (David Cooke, private communication).

In a magnetised plasma, calculating the current-voltage relation for even a simple sphere is very complicated, and few really useful closed-form results exist. In contrast to NASCAP, POLAR can model the trajectories of the attracted ions taking magnetisation into account, but the effects seen when including non-zero magnetic field in the Freja simulations are found to be small, as could be expected. The gyroradii of the attracted ions are greater than the typical spacecraft dimension (about 1 m). For the repelled electrons, an analytical OML result is valid even in a magnetised plasma, and magnetisation can thus generally be neglected for the repelled species. An exception would be the case where a magnetic field line is cut at two points by spacecraft structures, with plasma open to space in between. However, as discussed below in subsection 4.5.6, magnetisation may possibly have impact on emission of photoelectrons and secondary electrons.

4.5.1.3. Photoelectron emission

Photoelectron emission from surfaces exposed to sunlight provides an important current in the charging balance for a spacecraft in geostationary orbit or elsewhere in the tenuous magnetospheric plasma. At Freja altitudes, the photocurrent is not as important as in the GEO environment, although it acts to stabilise the spacecraft potential in sunlit conditions. The photocurrent from a surface is fairly simple to model, at least as long as magnetisation effects are neglected. For negative potentials, the photocurrent is essentially independent of the potential: all electrons escape from the surface. This may be changed by the presence of a magnetic field, which may turn some photoelectrons back to the spacecraft even if they are energetically allowed to escape. Laframboise (1988) found that for a planar surface with an angle θ between the surface normal and the magnetic field, the current carried by emitted electrons decreases by a factor $\cos\theta$ if there is no normal electric field at the surface. If such an electric field is present, the quenching effect becomes less important, and for high voltage charging, here defined as a high value of the ratio of the *E/B* drift speed to the particle speed at emission, the effect is negligible. Still it may be important for low-level charging events. POLAR presently does not include this effect.

Another effect suppressing the photocurrent is the formation of electrostatic barriers due to different voltages on different surfaces on the spacecraft, as illustrated in Figure 4.5-1. Local potential minima may form in space outside a surface, turning back photoelectrons to the surface. POLAR 1.3.7. includes a simple model of this phenomenon (see subsection 4.5.6), known to be important in charging in geostationary orbit conditions (Purvis, 1983) where the plasma density is low.

The electrostatic field may also return emitted particles to other points on the spacecraft than they were emitted from. These photoelectrons should be accounted for in the current balance also for the surface where they end up. This phenomenon is incompletely modelled in POLAR 1.3.7. (see subsection 4.5.6).

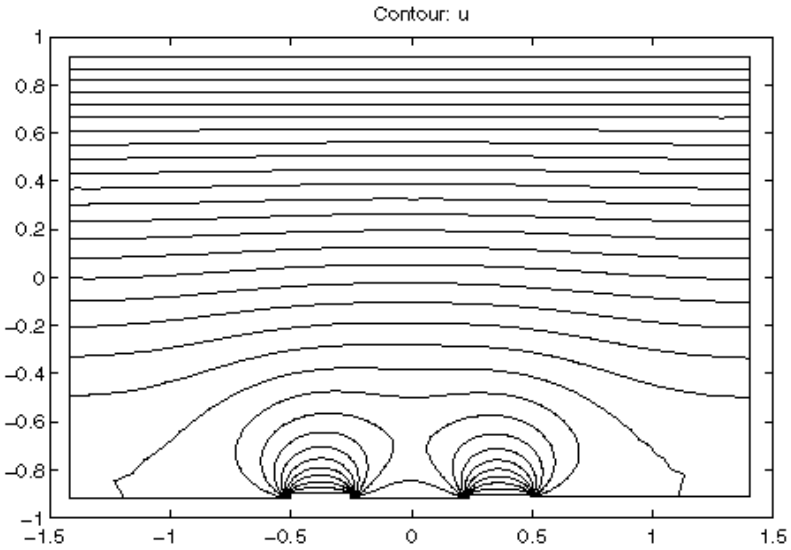

Figure 4.5-1. A numerical solution of the two-dimensional Laplace equation above a surface at 20 V with two small segments at 30 V. Equipotential lines with 2 V separation are shown. The potential is put to zero at the upper boundary, and the horizontal electric field is zero on the right and left boundaries. The formation of a local potential maximum of a few volts in space between and above the two small plates at 30 V is evident. Such a potential can form a barrier for particles expelled from the surface between the two small plates with energy below the magnitude of the potential barrier.

4.5.1.4. Secondary electron emission

When an electron or ion hits a surface, one or several other electrons may be emitted from the material, usually at fairly low energy (a few eV). The number of electrons emitted for each incoming particle is known as the yield Y. For incoming electrons, Y strongly depends on their energy E. The yield curve $Y(E)$ is obviously zero for zero energy and also zero for infinite energy (as very high energies give very limited possibility of interaction),

so there must be at least one maximum in between. Experimentally, most materials are found to have one maximum in the yield curve, at a few hundred eV (compare Figure 4.5-3, below). The maximum value of *Y* may well exceed one: for aluminium, the peak yield is 0.97, while it is around 3 for teflon. Thus secondary electron emission may be very important to the current balance for a spacecraft. A corollary is that simulations and calculations of spacecraft potential will be sensitive to errors in the model used for describing the secondary emission.

POLAR includes the NASCAP algorithms for calculation of secondary currents. The inputs needed are material properties and spectra of incoming primary particles. All materials known to NASCAP are included in POLAR, and for this study a number of other material specifications provided by ESTEC have also been used. As is the case with photoelectrons, POLAR looks at the secondary electrons only as a term in the current balance: they are not tracked out in space and do not contribute to the calculated charge density in the plasma. The treatment of current suppression due to potential barriers is similar to the that applied to photoelectrons.

4.5.1.5. Charging dynamics

Dynamic effects may enter the spacecraft-plasma interaction on two levels. The first and simplest level is when the boundary conditions in the plasma or for the spacecraft change so slowly that the sheath appears constant to the particle on a time scale it traverses the sheath. Dynamic effects on this time scale can be treated by introducing a displacement current in equation (4.5.1), thus requiring knowledge of the relevant capacitances. This can be a complicated task, as unless all parts on the spacecraft are conductors in contact with each other, there will be internal capacitances within the spacecraft. The spacecraft-plasma interaction may in this situation be modelled as a sequence of quasi-steady states, which is the approach taken by NASCAP and POLAR. The internal capacitances between various parts of the spacecraft must be explicitly provided by the user, while external capacitances to the plasma are modelled by the code.

The second and more advanced level for treating dynamical situations would be to consider not only quasi-steady states but the real dynamics of the plasma itself, down to Debye length and plasma oscillation scales in space and time. This would allow the modelling of wave generation and other time-dependent plasma phenomena, but would require a full plasma simulation of the interaction, which would be very costly in terms of computer power.

Correct treatment of charging dynamics including internal capacitances may be very important when studying the formation of differential charging on a spacecraft, which eventually may lead to an arcing discharge. Our main interest is the final equilibrium state of the overall satellite potential configuration, and we therefore do not attempt to model the charging dynamics. In particular, no attempt to estimate internal capacitances has been made. For numerical reasons, a short timestep has to be used in the simulations, but we do not attempt to interpret the timescale we use as necessarily corresponding to the real charging timescale. One may note, however, that the charging timescale for Freja is

observed to be short. Figure 4.3-2 indicates that the variations of the spacecraft potential, as mapped by the low energy cutoff in the ion spectra, occurs on a timescale of a few seconds, which is confirmed by investigations of individual ion spectra with a 2.8 second time resolution.

4.5.2. Modelling the Freja spacecraft

4.5.2.1. General Freja design

Freja is a sun-pointing spacecraft with solar panels placed on a flat circular surface. The overall diameter is 2.2 m (Figure 4.5-2). The solar panel platform constitutes the "upper" deck or platform. The "lower" deck is connected to the upper via a central aluminium tube. Radially from this tube four support webs are mounted between the decks. The lower deck is 1.2 m in diametre. The distance between the two decks is 0.44 m.

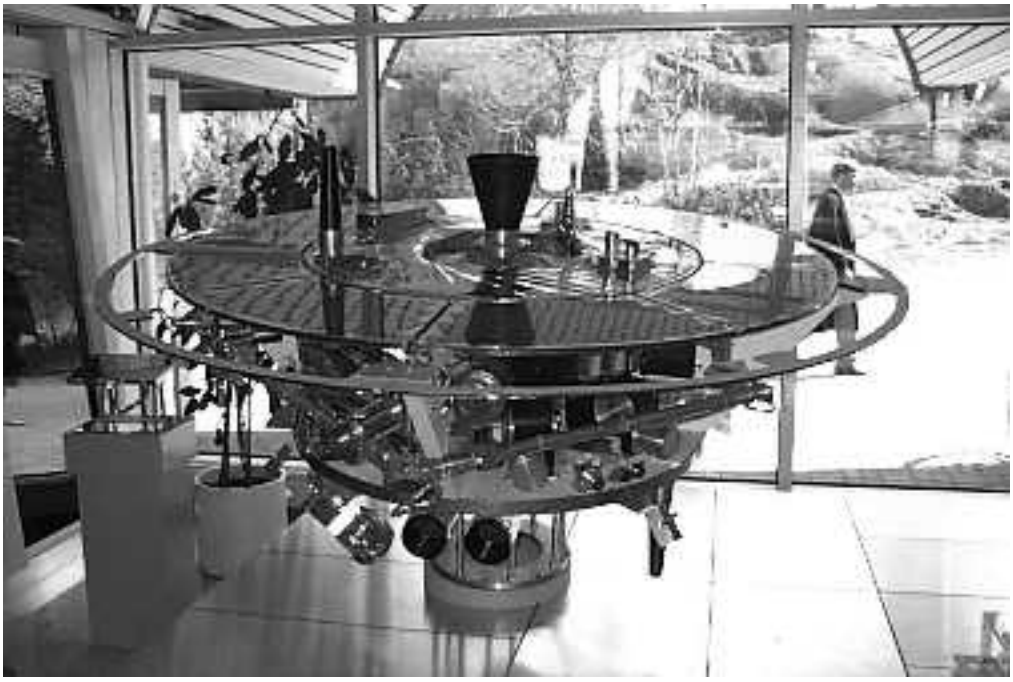

Figure 4.5-2. The Freja mockup at the entrance hall of the Swedish Space Corporation in Solna, showing the essential features of the spacecraft. The flight model has the instrument bays covered by thermal blankets.

In the central tube two solid powered motors, used to lift the the spacecraft into its final orbit, are mounted: one facing "upwards", one facing "downwards". Each motor has a nozzle made of composite material. The conductive properties of these nozzles, which are dielectrics on ground, are not well known, but a carbonisation effect during their use is assumed to make at least their inner surface conductive. We have in this study represented them by the conductive material CFPR (see next section) and a variation of this material with very low conductivity. The space between the decks is partitioned by

the support webs into four distinct compartments known as instrument bays, where the different booms, scientific instruments and other system units are mounted.

An important design goal was to have as much as possible of the outer surface electrically conductive in order to cancel electrical charges induced by the plasma environment and prohibit differential charging. It is not possible to achieve a 100% coverage of the surface with conductive material, as insulating material must be used for certain purposes, such as insulating an electrostatic probe from the satellite. The total area of exposed insulators on Freja is about 0.38 m^2 (including engine nozzles) which may be compared to the thermal blanket exposed area of about 5.5 m^2.

The basic structure of the spacecraft is made of aluminium. Structure elements extending outside blankets are painted with white conductive paint of type PCB-Z. The eight identical solar panels are each covered by solar cells of 0.19 m^2 area, giving a total solar cell area of 1.52 m^2. A transparent conductive coating of indium tin oxide (ITO) is applied to the solar panels in order to ensure conductivity.

To keep the temperature within desirable limits, and to provide a conductive outer coating, a large part of the spacecraft including most of the instrument bays are covered by Sheldahl thermal blankets of aluminised kapton with ITO coating (Sheldahl, 1985).

4.5.2.2. Freja surface materials

In order to accurately model the spacecraft, we must know the properties of its surfaces. A detailed investigation of the Freja satellite has been performed, and a materials list has been compiled. A summary of the surface materials is found in Table 4.5-1. Names of model materials for the POLAR simulations are also given in the table. These model materials are further discussed below. For purposes of spacecraft charging, the exposed insulators are of particular interest. These are listed in Table 4.5-2.

For correctly calculating the charging and discharging of dielectrics and the photocurrents and secondary currents, POLAR needs a specification of the material of each surface in the spacecraft model it uses. The principal properties we need to know for each material are the relative dielectric constant, the thickness of dielectrics, the bulk conductivity and surface resistivity, the atomic number, parameters describing the secondary yield curves for incoming ions and electrons, the maximum photocurrent and the discharge potentials. Laboratory values of these parameters for some materials are available directly in the NASCAP and POLAR codes. Other material parameters have been supplied by ESTEC based on measurements at DERTS. For the POLAR simulations of Freja charging events, the following materials have been used to model the satellite:

ITOC Indium tin oxide (ITO) coating. The secondary electron yield for materials with this coating has in laboratory tests been found to be rather independent of the underlying bulk material. In our case, the ITOC is applied on the solar panels.
Source: ESTEC

BLAN Thermal blankets of Sheldahl fabrication. Aluminized kapton with ITO coating.
Source: ESTEC

ALUM Aluminium for some spacecraft structure parts, particularly interface ring. The values we use are for pure aluminium surfaces. In reality, oxidization will increase the secondary electron yield. Source: NASCAP.

PCBZ White paint assumed conductive in space, applied to most aluminium areas which otherwise would have been directly exposed. Source: ESTEC

CFRP Conductive carbon fibre material, used to model the engine nozzles and some details. Source: ESTEC

CARB This material has been constructed for simulating the behaviour of non-conductive carbon fibre. We use the parameters for CFRP above, with bulk conductivity and surface resistivity replaced by CONT values.

CONT A generic for dielectric materials having been exposed to the space environment. In laboratory tests, the secondary yield properties were found to be rather independent of which dielectric it was, so we use this for modelling of all dielectrics except carbon fibre parts. Source: ESTEC

Part	**Material**	**Model material**	**Area [m^2]**	**Comment**
Instrument bays	Thermal blanket	BLAN	2.8	Thermal blankets covering scientific instrument electronic units and system units. Some exposed detectors.
Top and bottom platforms	Thermal blanket	BLAN	2.7	
Solar panels	ITO coating	ITOC	1.65	
Central tube inner mantle	Thermal blanket	BLAN	1.1	
Support webs (four)	Painted aluminium	PCBZ	4 x 0.7	Only exposed outer parts are painted and included in the area estimate.
Interface ring	Al	ALUM	0.5	Approximated as 2D ring, r = 1100 mm, dr = 37 mm
Main engine STAR 13A body	Titanium	ALUM	0.4	Considered as mantle of cylinder r = 154 mm, h = 396 mm.
Solar cell support	Painted aluminium	PCBZ	< 1.65	Some area covered by support webs and bay blankets.
Sun sensors	ITO coating	ITOC	2 x 0.05	One on top, one on bottom platform. Approximate dimensions 0.1 x 0.1 x 0.1 m.
TM antennas	Carbon fibre	CARB	2 x 0.05	One each on top and on bottom platform. Considered as cylinder r = 50 mm, h = 340 mm. Assumed insulator in this study.
Main engine nozzle	Carbon fibre	CARB	0.3	Considered as cylinder of radius 150 mm, h = 240 mm. Assumed insulator in this study.
Bottom engine STAR 6B	Aluminium	ALUM	0.02	

Table 4.5-1. Materials of major exposed surfaces on Freja. The "model material" refers to the baseline input for POLAR simulations.

Item	**Surface area** [m^2]
External parts of equipment bay:	
LSL Coax	0.0001
Separation switch harness	0.0300
Coax switches	0.0036
Power splitter	0.0009
Coaxes	0.0144
TICS cable	0.0020
Arming plugs	0.0020
DC-magnetometer boom:	
DC probe harness	0.0023
Cable loops	0.0075
CYLP pyro	0.0018
Search Coil Magnetometer boom:	
HF pyro	0.0018
Bottom platform:	
Lower TM antenna cover	0.05
S-band antenna coax	0.0050
Kevlar retention string	0.0004
TESP cradle rubber	0.0006
TESP rubber support	0.0010
TESP cables	0.0050
TESP backshell	0.0020
TESP pyro	0.0015
TESP kevlar string	0.0004
LSL antenna base	0.0015
MATE cable	0.0045
MATE cradle support	0.0004
STAR 6B nozzle	0.0100
Top platform:	
Upper TM antenna cover	0.05
S-band antenna coax	0.0050
Kevlar retention string	0.0004
STAR 13A nozzle	0.1200
STAR 13A harness	0.0150
Solar panels:	
Brackets	0.0058
Rear side cabling	0.0110
Top side TCC	0.0180
Edge TCC	0.0285
Total area including nozzles:	**0.38**
Total area excluding nozzles:	**0.24**

Table 4.5-2. List of exposed insulators on Freja. The list also includes the engine nozzles, as the impact of a possible non-conducting layer on these is assesed in the study.

The most important feature of the materials for this study is the secondary electron emission (Figure 4.5-4). This also shows the yield curves for another conductive paint CPAI (source: NASA) and for Teflon (source: ESTEC).

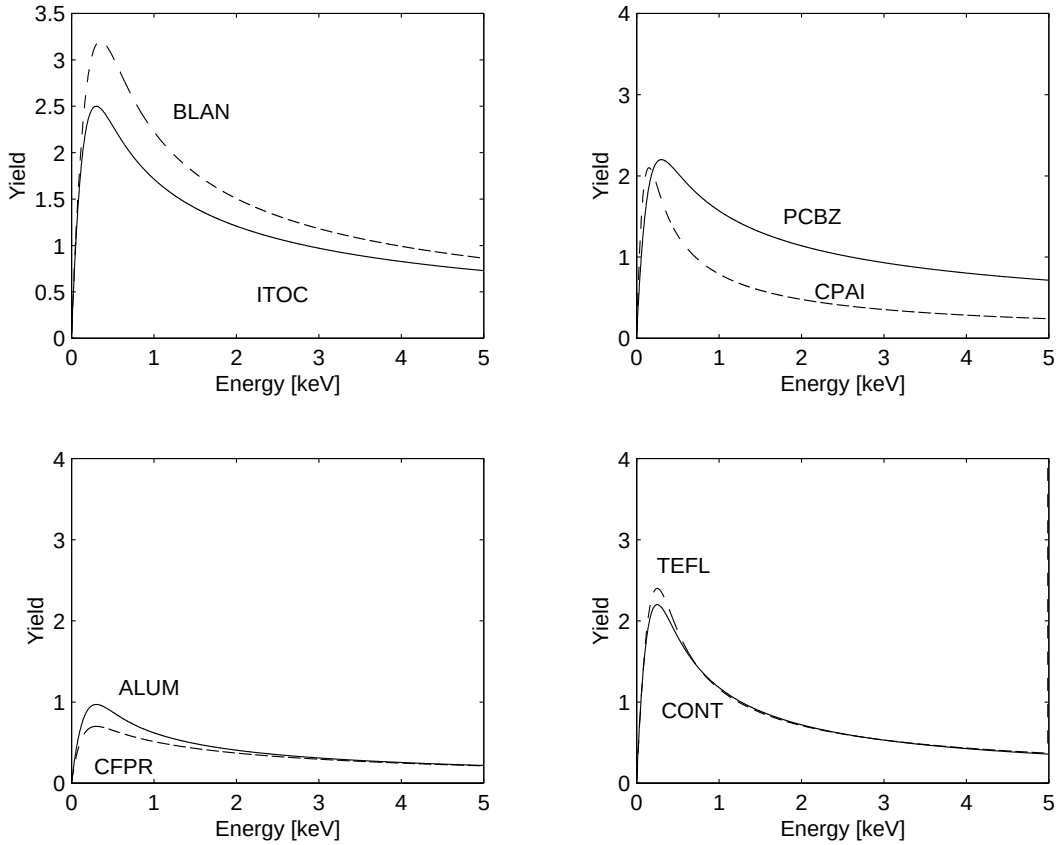

Figure 4.5-3. Secondary yield curves for materials used in the Freja model.

4.5.3 Freja models for POLAR simulations

In POLAR, a spacecraft is modelled in a fixed grid of cubical elements. Except for the additional ability of NASCAP to model one-dimensional structures (i.e., booms) as well as the two-dimensional (rectangular plates and slanted triangular surfaces) and three-dimensional (cuboids, octagons, wedges etc) objects possible to model in POLAR, the two programs are similar in terms of spacecraft definition. For a detailed description of how to model a spacecraft in POLAR, see PUM sections 6.10–6.14.

In order to test the effects of geometric details in the simulation software, spacecraft models on three levels of sofistication have been used. The basic versions of these three models, known as A, B, and C in order of increasing geometric complexity, are outlined below. In the actual simulation runs, the models have been varied in terms of material definitions and slight geometrical changes in order to estimate the effects of such changes. The models are shown in Figures 4.5-4 – 4.5-6.

Model A is a simple definition of the spacecraft as a rectangular object of 2x1x2 grid units (Figure 4.5-4). This very simple model is used (a) for testing the plasma environment models on a simple object requiring comparatively little computational effort, and (b) for comparison to the results from Model C in order to test the effects of geometrical details and small surfaces of non-conducting materials.

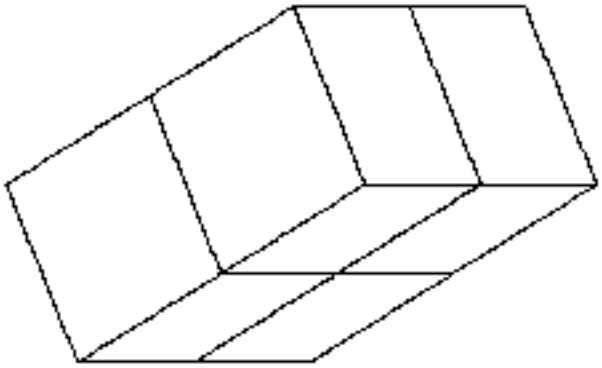

Figure 4.5-4. Geometry of Freja model A.

Model B uses a spacecraft definition grid size of 17 x 17 x 33 cells, which was the limitation of previous versions of POLAR. This leads to a grid unit length of approximately 16 cm for Freja. A version of this model was first used in preliminary runs in May 1997 (Svensson, 1997), and later for comparisons to Models A and C for some events. The model incorporates the main features of Freja (Figure 4.5-5) with some details.

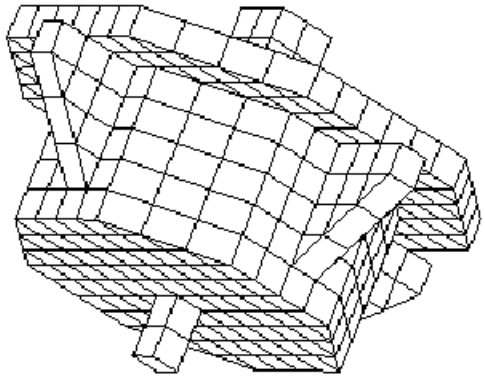

Figure 4.5-5. Geometry of Freja model B.

Model C is the most detailed, with a grid size of 10 cm, allowing additional detail (Figure 4.5-6). In particular, implications of adding small objects of insulating material are possible to study in this model. For more details of these models, see SPEE-WP120-TN, available at the SPEE www-server: http://www.geo.fmi.fi/spee/docs/

POLAR 1.3.7 allows a grid size of up to 50 x 50 x 100 points for the definition of the spacecraft. However, a maximum number of 1250 simple surfaces can be handled, which means that for any reasonably spherical or disc-like spacecraft, the full number of grid points can never be used. For Freja, with a diameter of 2.2 meter, geometrical restrictions alone would allow a resolution of less than 5 cm in grid size, but due to the need

to keep the number of surface elements low, the grid resolution of 10 cm used in Model C is the smallest that can be used in practice.

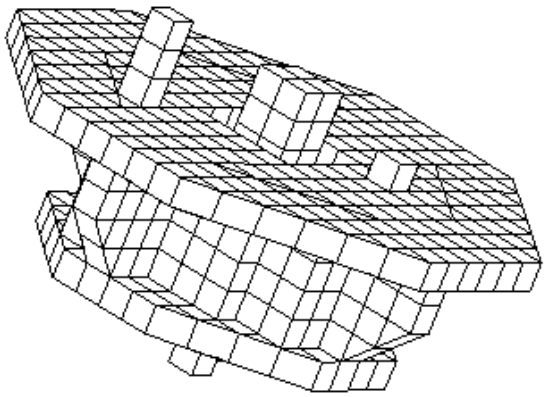

Figure 4.5-6. Geometry of Freja model C.

Figures 4.5-7 and 4.5-8 show examples of how the materials described above have been distributed on spacecraft models A and C. For model C, care has been taken to get the total area of the insulators as closely approximating the values in Table 4.5-2 as possible. For the crude model A, the dielectric surfaces are exaggerated in size. More examples can be found in SPEE-WP120-TN.

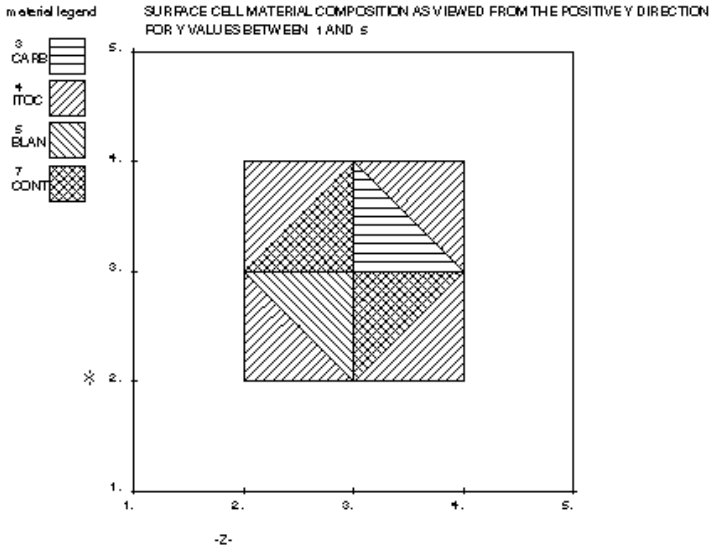

Figure 4.5-7. Distribution of materials on the upper deck and solar panels in model A.

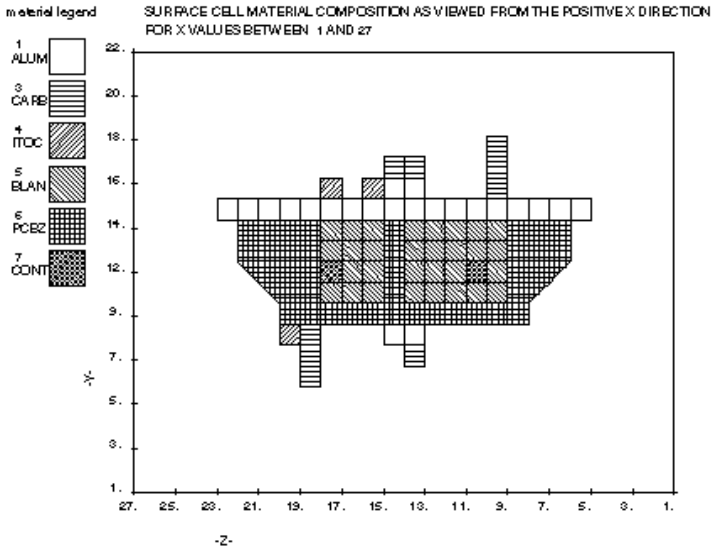

Figure 4.5-8. Distribution of materials on the sides of model C.

4.5.4. Modelling the charging environment

The spacecraft-plasma interaction depends on the actual plasma parameters. The cold plasma density and temperature define the fundamental shielding properties of the plasma and the plasma currents to the spacecraft. We also need to know the ion composition, as the currents depend on particle dynamics. In auroral conditions, charging is caused by auroral electrons, so we must also characterise the energetic electron environment. Additional information on sunlight/eclipse conditions and magnetic fields is also sometimes required, as is the orbital speed of the spacecraft.

For the simulations presented here we have, unless otherwise stated, assumed that the only ion species present is oxygen, and that ion and electron temperatures are equal. Including a component of hydrogen, which is likely to be present in reality, has the effect of decreasing the observed charging level as the lighter hydrogen is easier for the spacecraft to collect. The spacecraft speed is always put to 7 km/s, and the magnetic field is specified at its observed value and direction. However, the effect of satellite spinning is not included, so one particular spin phase value is picked at random.

The precipitating auroral electrons are in POLAR modelled as a sum of a power law, a hot Maxwellian and a Gaussian population. The particle flux expression
[unit: m^{-2} eV^{-1} $sr^{-1}s^{-1}$] is

$$\Phi(E) = AE^{-\alpha} + \frac{n}{\sqrt{2\,m_e}}\frac{E}{(\pi K T_2)^{3/2}} e^{-\frac{E}{KT_2}} + BEe^{-\frac{(E-E_0)^2}{\delta^2}} \qquad (4.5.2)$$

(PUM section 3.41) where A, α, C, T_2, B, E_0 and δ are free parameters that may be fitted to a measured distribution. The form of (4.5.2) is inspired by a statistical study of auroral zone electron spectra by Fontheim et al. (1982). Although not perfectly flexible, we will see below that it actually can be used to get good fits to the electron spectra en-

countered by Freja in the events to be studied here (e.g. Figure 4.5-9). The distribution is mapped to a surface element on the spacecraft by use of energy conservation and Liouville's theorem, and the resulting current contribution is calculated by integration over energy. The Maxwellian and Gaussian components have analytic expressions for the integration over all energies, but for the power law component finite integration limits must be supplied since the integral diverges at zero energy.

One should note that in order to find the parameters in equation (4.5.2), we cannot directly compare to the electron spectra observed in the charging events. These refer to electron energy as measured at the spacecraft, which in charging events is not the same as the electron energy of unperturbed plasma. We have therefore corrected for the observed charging level by mapping the POLAR flux expressions from the outside plasma to the spacecraft using Liouville's theorem.

Expression (4.5.2) includes no reference to angular distribution, and POLAR assumes the distribution to be isotropic. While this is rarely the actual case, a high degree if isotropy is often observed in electron distributions at Freja outside the loss cone due to the isotropising magnetic mirror effect on particles travelling from the magnetosphere down toward the ionosphere. In some situations the anisotropy of electron spectra may be an important factor for spacecraft charging processes, but this will mostly apply to spacecraft with large non-conductive parts.

Typical plasma conditions for the Freja charging events were discussed in sections 4.3. and 4.4. For the simulations here we have also used additional detailed data. For determining the parameters describing the energetic electrons, we have visually fitted expressions of type (1) to electron spectra observed by TESP (Boehm et al., 1994) and/or MATE (Eliasson et al., 1994) electron detectors on Freja. Plasma density is inferred from the identification of plasma oscillations and Langmuir waves, in wave data from the F4 instrument (Holback et al., 1994). Observational Freja input on the electron and ion temperatures is weak, although T_e sometimes can be estimated from Langmuir probe sweeps of the F4 instrument if any reasonably interpretable sample is available close to a charging event. When no input is available, we assume 0.2 or 0.3 eV for ions and electrons alike.

4.5.5. Simulations of charging events

4.5.5.1. Event selection and characteristics

Out of the ten events studied in detail in this project, five six-second periods (a full spin revolution) were selected for detailed simulation of the spacecraft charging process using SUCHGR and POLAR. Table 4.5-3 summarizes the baseline environmental parameters, discussed in Section 4.5.4 above, used in the simulations.

Each event in Table 4.5-3 is studied during a full spin period, which is 6 seconds. The plasma density on line 5 is based on a plasma oscillation within this period. Electron and ion temperatures (lines 6 and 7) are assumptions, except for event 9 where the electron temperature has some experimental foundation. Line 8 is the electron Debye length, line 9 the oxygen-based Mach number of the plasma flow seen in the spacecraft frame of

reference, and line 10 is the assumed fraction of oxygen ions. Lines 11 to 19 are parameters defined by equation (4.5.2.), based on visual fits of observed electron spectra (pcutl and pcuth are the integration cutoffs). Two examples of such fits are presented in Figures 4.5-9 and 4.5-10. Lines 20 and 21 show magnitude and direction, in the spacecraft frame of reference, of the observed magnetic field. As the satellite is spinning around the y axis in our models and we consider spin averaged quantities, the direction of B in the x-z-plane is undefined. However, the angular relation between the directions of magnetic field, direction to sun (line 23) and plasma flow direction (line 24) are fixed, and we have arbitrarily chosen a spin phase angle such that the plasma flow is in the y-z-plane in all our simulations. Line 23 is the solar intensity, defined as 0 in darkness and 1 in full sunlight. An observed value of the spacecraft potential in this six second interval, as based on ion data (Section 4.2.5), is found on line 25.

1	Event #	3	6a	6b	7	9
2	Orbit	790	1666	1666	1785	736
3	Date [yymmdd]	921205	930209	930209	930218	921201
4	UT [hhmmss]	023828	091715	091800	093148	003508
5	n_e [cm^{-3}]	125	50	30	60	125
6	T_e [eV]	0.3	0.2	0.3	0.3	2
7	T_i [eV]	0.3	0.2	0.3	0.3	0.5
8	λ_D [m]	0.4	0.5	0.7	0.5	0.9
9	M_{O+}	5.2	6.4	5.2	5.2	4.0
10	n_{O+}/n_e	1	1	1	1	1
11	n_2 [m^{-3}]	1.5e3	2.2e5	6.2e5	5.2e4	1.3e4
12	T_2 [eV]	5e3	7e2	8e3	2.9e3	4e2
13	A [m^{-2} sr^{-1} s^{-1} eV^{-1}]	3.2e12	1.9e11	7.6e14	3e12	3.1e11
14	α	1.9	1.3	2.0	1.6	1.3
15	pcutl [eV]	0.5	0.5	0.5	0.5	0.5
16	pcuth [eV]	6.5e4	1e4	2e4	2e4	6e4
17	D [m^{-2} sr^{-1} s^{-1} eV^{-1}]	1.2e5	3e4	1.3e4	1.5e3	6e4
18	E_0 [eV]	1.5e3	2e3	1.1e4	1.3e4	1.8e3
19	δ [eV]	3e3	6e3	1.5e3	8.1e4	6.5e3
20	B [μT]	26	28	28	28	27
21	B direction (x,y,z) (model B)	0.1 -0.62 -0.78	0.55 -0.83 -0.02	0.55 -0.83 -0.02	0.76 -0.63 -0.19	0.71 -0.69 -0.14
22	Solar intensity	0	0	0	1	0
23	Sun direction (x,y,z) (model B)				0.12 -0.88 -0.46	
24	Flow direction (x,y,z) (model B)	0 -0.70 0.72	0 0.26 0.97	0 0.26 0.97	0 -0.21 0.98	0 -0.06 1.00
25	Observed potential [V]	-25	-40	-1000	-160	-40

Table 4.5-3. Freja charging event parameters for modelling by SUCHGR and POLAR. The table entries are described and discussed in Section 4.5.5.1.

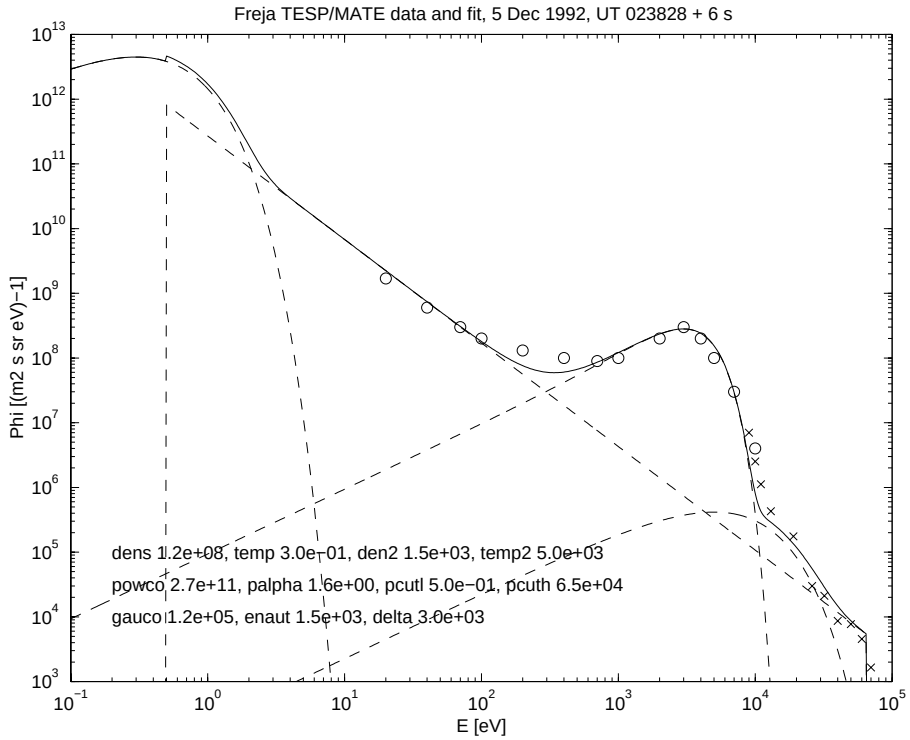

Figure 4.5-9. Spin-averaged electron spectrum for event 3 (orbit 790) based on data from the Freja TESP (o) and MATE (x) electron spectrometers, and a fit to the flux expression (2) with parameters as given in table 4.5-3.

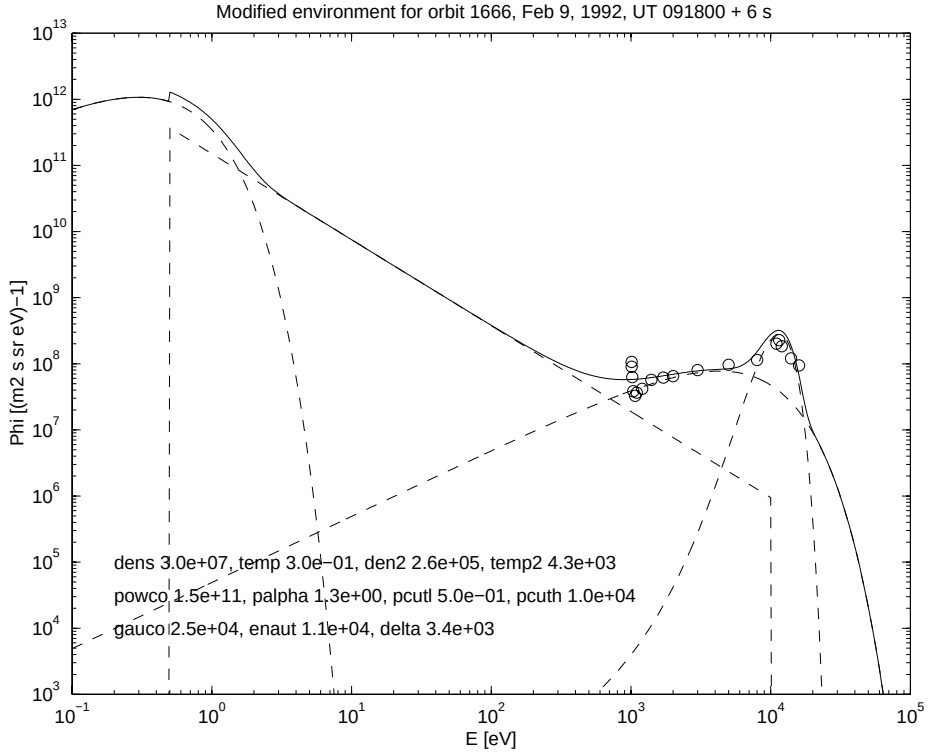

Figure 4.5-10. Spin-averaged electron spectrum for event 6b (orbit 1666) based on data from the Freja TESP (o) electron spectrometer, and a fit to the flux expression (2) with parameters as given in Table 4.5-3.

4.5.5.2. Event simulations

After having defined the spacecraft model and the plasma model, we have a well-defined problem for the SUCHGR and POLAR codes. Table 4.5-4 summarizes the results we get when using this direct approach on the problems. Some of the table entries are based on orbit limited and some on space charge limited calculations, depending on the nature of the problem. A more detailed disucssion of each case is found in SPEE-WP120-TN.

In most cases the simulations did not reproduce the observed charging levels. Only one case, event 9 using the simple model A produced high charging level, this case actually exceeding the observed level. However, when the more realistic model C was used, also here only weak charging was found. The reasons for these discrepancies are disucssed below.

Event	3	6a	6b	7	9
Highest observed voltage	-65	-1800	-1800	-500	-70
Observed voltage at modelled time	-25	-40	-1000	-160	-40
SUCHGR (ITOC)	-0.8	-0.1	-0.3	2.6	-0.6
SUCHGR (ALUM)	-7.2	-12	-72	2.9	-12
POLAR (model A)	-6.9	-5.4	-11	[-4…1]	-105
POLAR (model C)	-1.2	-18	[-40…0]	[-0.2…0.9]	-1

Table 4.5-4. Results of SUCHGR and POLAR simulations for the nominal environments defined in Table 4.5-3. Model A has 1 m grid size, model C grid size 10 cm. Table entries are potentials in volts. The brackets denote that oscillations within these limits were found when the simulation was stopped after it had become clear that charging to the observed level was not going to be reproduced even if the oscillation would damp out.

4.5.5.3. Discussion of the simulation results

There are several possible sources for the observed discrepancy between the observed charging voltages and the POLAR predictions. They may be grouped into (a) errors in the spacecraft definition, (b) errors in the plasma environment definition, (c) errors in the application of the code and (d) limitations of models used in the code. A fifth possibilility, namely pure software bugs, is considered less likely as POLAR has been extensively tested for other situations and showed to work there. We discuss each of these possibilities below.

(a) *Spacecraft definition.* For all the major materials on Freja, we have used parameters established in the laboratory. The exception are the relatively small areas of the nozzles and TM antennas, for which we have assumed material parameters as for CFRP but with very low conductivity, and the also small aluminium parts, for which we have used unoxidized aluminium as model. However, defining the carbon fibre areas as CONT or CFRP has been found to make no big effect to the simulations, and the use of pure alu-

minium parameters should exaggerate rather than diminish the predicted charging level as the secondary electron yield increases in the oxidization process. If something should be wrong in the material description it must be for some of the more dominating Freja surface materials. One may note that Freja charging events are seen from the very beginning of the mission, so material ageing is a less likely cause of the discrepancy. It is outside the scope of this study to experimentally or theoretically investigate the properties of the materials used. As an example one may note that if the assumed high conductivity of the PCB-Z paint should be significantly lower than thougt, this would bring a major change to the spacecraft model, making a major part of the spacecraft an effective dielectric. Another such possibility is that the ITO cover on the thermal blankets may crack and decrease conductivity. Such effects could cause build-up of large differential charging levels, which by influencing the potential distribution in plasma and hence particle orbits may cause an overalla charging of the spacecraft.

Spacecraft model problems could also be in the geometry of the spacecraft. An even more detailed model of the spacecraft may possibly give better results. We think this is less likely, as it all major parts are quite accurately modelled by model. Although we do not think it likely, it is in principle possible that some of the larger linear elements on Freja, like the magnetometer booms, could influence the potential distribution and thereby change the charging level. One further study could thus be to construct a Freja model for NASCAP, which can handle booms. Although NASCAP cannot accurately model the auroral spectra seen by Freja, a comparison between NASCAP and POLAR results for a charging environment they both can handle could be of interest.

(b) *Plasma environment*. Several of the plasma parameter values we have used are rather uncertain. For the cold plasma, the temperatures we have used are assumed values. However, varying these within reasonable limits does not very much change the voltage predicted by POLAR. Taking event 3 as an example, runs on model C with temperature 0.1 eV and 1 eV yield spacecraft potentials of –1.3 V and –3.8 V, respectively, which are not dramatically different from the –1.2 V observed for the nominal parameters. We do not think that the cold plasma density could be a major source of error. First, the density values in these charging events are already very low for this altitude range. Second, our identification of the narrowband HF emissions on which we base our density estimates as plasma oscillations and Langmuir waves has been verified by comparison of these emissions with the Langmuir probe current in non-charging events. Third, the ion spectra in the charging events show an uplift in energy of the ram flow, not a major decrease of the ram flow intensity, which should be the case if the density dropped drastically.

The high-energy electrons are well measured by the TESP and MATE detectors, who have been tested in numerous studies (e.g. Boehm et al., 1994; Eliasson et al., 1994). In the region of overlapping energy the two detectors give very similar shapes of spectra with intensities within factor of two from each other. However, we should note a few possibly important uncertainties. First, in the events studied, no truly field-aligned electron spectra have been obtained. The pitch-angle coverage of the detectors depended on the spacecraft attitude. The perpendicular direction is always covered, but pitch angles

below 20° were not covered in any of our cases. Table 4.5-5 summarizes the pitch angles of the spectra used, and the observed anisotropies. In some cases, there is no sign of anisotropy in the pitch angle range covered (events 7 and 9), while others may show such anisotropies, in particular for the energy range around 1 keV, which has important impact on the secondary electron production. For the modelling, the 90° spectra have been given more attention, as in an averaging process to find the omnidirectional flux, the directional fluxes will be weighted by the sine of the pitch angle. However, we should note that there in principle may be energetic electrons at near-parallel or near-antiparallel pitch angles which we do not measure. This cannot be checked within the Freja events used here. An extended study could search for Freja charging events with better pitch angle coverage, or use another data set with more complete pitch angle coverage most of the time. Even so, the only way to include them in a POLAR 1.3.7 simulation would be to use pitch-angle averaged spectra.

Event	**Available P/A** [°]	**Anisotropy**	**Used P/A** [°]
3	68, 69, 84, 100	Peak value (3 keV) factor 2 higher at 68° than at 90°.	68
6a	33, 34, 90, 103	Peak value slightly higher at 90°. Flux at 1 keV factor 4 higher at 90° and 103° than at 33° and 34°.	90
6b	32, 33, 90, 104	Peak isotropic. Factor 2 higher flux at 1 keV (uncorrected) than at 32° and 33°.	Average
7	22, 23, 90, 103	Isotropic	-
9	44, 46, 88, 93	Isotropic	-

Table 4.5-5. Observed anisotropies in the spectra used for the specification of the nominal electron environments for the modelled charging events. All energies are as observed at the detector without any charging correction.

(c) *Application of POLAR*. The POLAR code is a complex numerical package with several options on the use of physical and numerical models and of numerical parameters. A straightforward application of default settings of the code fore several of these parameters could lead to unphysical results. A good example is the choice of the grid size. For the Freja applications in plasmas of low density, the real sheath size may easily extend outside the chosen simulation box edge. In that case, the sheath predicted by the code would be too small, the ion currents underestimated, and the magnitude of the charging level overestimated. While this is easy to detect, a more subtle effect is that even though the sheath boundary is well inside the simulation box, the boundary condition that the potential is zero one grid unit outside the simulation box could cause errors in the potential determination, and thereby in other parameters like the sheath location an in the prediction of barrier potentials.

While care has been taken to find an minimise such sources of error, investigating all aspects of the POLAR code is a formidable task beyond the scope of this study. However, the results presented here are based on extensive trial-and-error investigations and studies of parts of the code.

At least in one of the simulation cases (6a) the initial condition on potential was very important for the final outcome. This raises the question whether the time history of charging should be modelled as well. This could, in principle, be done with POLAR 1.3.7 but would, in practice, require an effort that was not possible with the available resources for this study.

(d) *Code limitations.* POLAR has previously been used to simulate DMSP charging events, where higher plasma density was reported. The low plasma density in the Freja events makes sheath sizes large, which is a practical problem in a code using the fixed-grid-resolution strategy of POLAR, leading to unreasonable simulation times. The simulations of our study required run times from one hour (model A) to a few days (model C) in a relatively fast workstation. Nevertheless, simulations performed using NASCAP as well as POLAR for a –80 V charging event (Svensson, 1997) indicated that the sheath size limitation of POLAR cannot explain the discrepancies between simulations and observations, as NASCAP was not more succesful in the case studied.

In addition, three of the five events studied here, and most of all observed Freja charging events, consider spacecraft potentials less than –50 V, while the driver for the development of POLAR and other charging codes is the study of higher levels of charging, where potentially harmful effects in terms of arcing and discharging may set in if differential voltages appear. However, the biggest discrepancies between simulation and observations was seen to be in the highest charging level events.

In the following section, we discuss some physical phenomena that may need a refined treatment in the code in order to model the Freja charging.

4.5.5.4 Suppression of secondary current and photocurrent

It was above that a direct best-effort approach to POLAR modelling of the Freja charging events did not reproduce the observed charging levels. Possible causes for this discrepancy related to spacecraft and plasma modelling and code handling were discussed above. Assuming no such errors exist, what physical effects could cause the observed discrepancy?

The main problem for getting the observed charging level in a POLAR simulation is that the secondary currents, and for the sunlit event 7 the photocurrent, must be suppressed. From studies of spacecraft in geostationary orbit, it is well known that one way of efficiently doing so is the build-up of barrier potentials related to differential charging (e.g., Purvis, 1983). On Freja, such a scheme has its problems as the area of insulators is fairly small. On the other hand, the secondary yield of the carbon fibre elements (nozzle, TM antenna domes) are so low that they possibly may charge differentially to very high voltages. Indeed the freja simulations showsome development of differential charging. It

is therefore of interest to accurately model the suppression of secondaries and photoelectrons by barrier potentials.

The POLAR 1.3.7. algorithm for modelling this is rather simplistic. If the secondary current or photocurrent emitted by a surface is I_0 and the normal electric field E_n on the surface is such that the emitted electrons are attracted back to the surface, POLAR assumes that the actually escaping current is

$$I_{esc} = \frac{I_0}{1 - \Phi / U_0} \tag{4.5.3}$$

where $\Phi = 2E_nD$, D is the grid cell size and U_0 = 1 V. Figure 4.5-11 shows a comparison between this model and the suppression resulting if assuming Boltzmann distributed electrons emitted along the surface normal into a purely normal electric field with potential barrier height equal to F. Temperatures 1.5 eV and 3 eV are used, approximately describing photoelectrons and secondary electrons, respectively. It is seen that for small barrier potentials, up to some 3 V, the current suppression of photoelectrons is more pronounced by POLAR than by the Boltzmann model. For secondaries, the corresponding limit value is about 9 V.

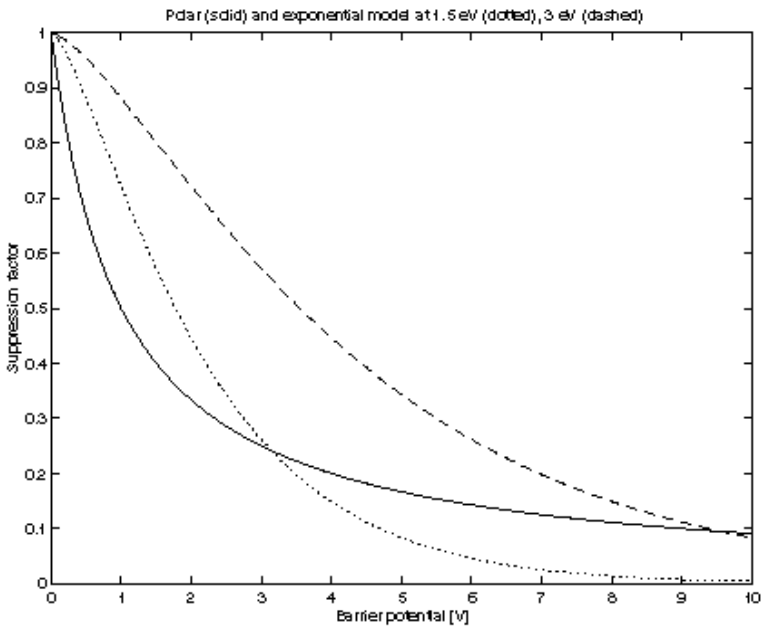

Figure 4.5-11. Comparison between the POLAR algorithm for suppression of photoelectrons and secondary electrons (solid curve) to a Boltzmann (dashed 3 eV, dotted 1.5 eV) with normal emission direction.

Neither the POLAR nor the Boltzmann algorithm takes higher-dimensional effects into account. For an infinite surface with a potential above it only depending on the coordinate along the surface normal, current limitation will be much more severe than modelled above if elctrons are emitted at all angles to the surface. On the other hand, the appearance of electric fields with a component perpendicular to the surface normal above the

surface on a geometrically complex spacecraft will allow some particles escape above other surfaces than those they were emitted from. Some particles will also hit the spacecraft at other surface elements that they were emitted from, a phenomenon called hopping. POLAR has a hopping model, unfortunately not supported in POLAR 1.3.7. This effect is therefore not included in the Freja simulations.

One may note that hopping and barrier formation are most effective in low density plasmas. In the charging situations previously studied with POLAR, densities have been higher and these effects therefore less unimportant (David Cooke, private communication). It may therefore be fair to say that the POLAR algorithms are not operationally validated for the Freja environment. In order to treat hopping secondaries and barrier suppression correctly on a geometrically complex spacecraft, numerical integration of test particle orbits in the self-consistently determined potential distribution around the spacecraft would be desirable.

Another means of achieving suppression of emitted electrons from a spacecraft surface may be by the ambient magnetic field turning them back to the spacecraft. This effect has been studied by Laframboise (1988) for infinite planes and for various strengths of the normal electric field at the surface. To estimate the maximum importance of this effect, we have integrated Laframboise's fitted expression for the current suppression as a function of angle between surface normal and magnetic field over a sphere. The result should give some average value roughly applicable to a spherical spacecraft as long as its radius is much larger than the gyroradius (the infinite plane assumption). The lower normal electric field, the more pronounced the effect will be. As an upper limit of the importance of the effect, we assumed Freja to be a sphere of radius 0.7 m with a vacuum (Coulomb) electric field around it. The results are tabulated in Table 4.5-6, showing that the effect possibly may be of some importance for the low-level charging events but certainly not for the charging to hundreds of volts, particularly as the real electric field will be stronger than the vacuum field, thereby diminishing the importance of this effect. However, for low-charging or floating potential calculations its impact on the photoelectrons may be of interest.

Event	**Iesc/I0**
3	0.85
6a	0.90
6b	1.00
7	0.98
9	0.90

Table 4.5-6. Lower bound on ratio of escaping to emitted secondary current (or photocurrent in the case of event 7) calculated by averaging the result of Laframboise (1988) over the surface of a sphere of radius 0.7 m assuming Coulomb electric field at the surface.

4.5.6. Conclusions of the charging study

A list of materials for the Freja satellite has been compiled. Properties for these materials are known from laboratory experiments, except for some details like engine nozzles and TM antenna domes whose properties are not well known. Models of Freja at different resolution have been prepared, and five Freja events were studied in detail to provide information on the plasma environment in the charging events. The models of spacecraft and plasma were used as inputs to simulations using the POLAR code. It was found vital to compensate the impact of the charging level of the spacecraft on the electron detectors when modelling the charging events for POLAR. The observed levels of charging were usually not reproduced by the code, although there were a few exceptions. For some events, the discrepancy is very large. Variations in cold plasma density and temperature within reasonable limits cannot explain the discrepancy. It is possible that high energy electrons at pitch angles not covered by the detectors could be responsible: however, the inverted-V precipitation spectra which accompany the charging events are usually quite isotropic except in the loss cone. The Freja model is quite detailed and should not be a cause of the discrepancy, although erroneous material parameters for some of the applied surface materials would be a problem if present. The numerical parameters for the code have been varied in numerous runs, and we do not believe unsuitable instructions to the code is a major error source, although this is hard to rule out using the POLAR documentation. Some physical processes not, or insufficiently, treated by POLAR may be the suppression of photocurrent and secondary electron current by potential barriers, hopping to other surfaces and, but only for the lowest charging voltages, the magnetic field, and effects of the charging history of the spacecraft.

When POLAR arrived in the late 1980s, it represented a major breakthrough in the study of charging effects in low Earth orbit in the auroral zone by its ability to self-consistently model a spacecraft sheath, include wake effects and magnetisation, and its facilities for modelling auroral electron spectra. Applications of POLAR have mainly concerned objects large compared to Debye length, which have shown that POLAR works well in this domain. The Freja situation, with the density so low that the Debye length is on the order of the spacecraft dimension, is something of a new application. If it is desirable to model this situation, we recommend that the Freja charging events are studied further as an input to code development. The Freja spacecraft and environment models used in this study are available for that purpose.

For the low-density plasmas studied here, the size of the sheath and the boundary condition that the potential should be zero at the simulation box edges sometimes are problems, as they neccesitate very large grids and thereby causes the calculation time to grow unpractically large. The possibility of employing some adaptive-grid algorithm at least outside the sheath should be considered, reducing the necessary grid resolution in this area and thus saving computational time without jeopardizing the physical accuracy.

The POLAR tools for keeping track of electrostatic barrier formation and currents hopping between surface elements may be insufficient for the Freja case, where these

features are of higher importance than in the denser plasmas studied in previous POLAR applications.

For low-level charging events and floating-potential calculations, the inclusion of a magnetic limitation algorithm for the secondary current and photoelectron current could be of some importance. Such an algorithm should be fairly straightforward to implement, using the interpolation formula of Laframboise (1988). If only the ability of the code to model high-level charging events (100 V or more in magnitude) is interesting, this effect may be neglected.